2014

Numerical Investigation Of Orographic Effects On Supercell Thunderstorms

Galen M. Smith
North Carolina Agricultural and Technical State University

NUMERICAL INVESTIGATION OF OROGRAPHIC EFFECTS ON SUPERCELL THUNDERSTORMS

Galen M. Smith

North Carolina A&T State University

A dissertation submitted to the graduate faculty

in partial fulfillment of the requirements for the degree of

DOCTOR OF PHILOSOPHY

Department: Energy and Environmental Systems

Major: Atmospheric Sciences

Major Professor: Dr. Yuh-Lang Lin

Greensboro, North Carolina

2014

The Graduate School
North Carolina Agricultural and Technical State University

This is to certify that the Doctoral Dissertation of

Galen M. Smith

has met the dissertation requirements of
North Carolina Agricultural and Technical State University

Greensboro, North Carolina
2014

Approved by:

Dr. Yuh-Lang Lin Major Professor	Dr. Ademe Mekonnen Committee Member
Dr. Yevgeniy Rastigeyev Committee Member	Dr. Jing Zhang Committee Member
Dr. Liping Liu Committee Member	Dr. Yuanfu Xie Committee Member
Dr. Keith Schimmel Department Chair	Dr. Sanjiv Sarin Dean, The Graduate School

Biographical Sketch

Galen M. Smith was born January 25, 1982 in Washington D.C., USA. He earned Associates in Applied Science in Computer Programming from Fayetteville Technical Community College in 2003. He matriculated to High Point University in 2004 and finished a Bachelor of Science in Mathematics with a minor in Computer Science in 2006. He continued his education at North Carolina Agricultural and Technical State University earning a Master of Science in Physics in 2008. He has continued at North Carolina Agricultural and Technical State University in the Energy and Environmental Systems Department where he is a doctoral candidate.

Acknowledgments

We would like to thank the National Oceanic and Atmospheric Administration (NOAA) Educational Partnership Program and the NOAA Earth System Research Laboratory for the use of their ZEUS supercomputer to conduct these simulations. Dr. George Bryan and NCAR are appreciated for allowing us to use CM1 and NCL, respectively. We thank IGES for the use of their Grid Analysis and Display System (GrADS) plotting software. This research was partially supported by the NOAA Cooperative Agreement No: NA06OAR4810187, and National Science Foundation Awards AGS-1265783, HRD-1036563, and OCI-1126543.

Table of Contents

List of Figures

List of Tables

Abstract

Orographic effects on tornadic supercell development, propagation, and structure are investigated using the Cloud Model 1 with idealized bell-shaped mountains of various heights and geometries and a homogeneous fluid flow with a single sounding. In total, the variations of height and geometry yield 16 terrain configurations. It is found that blocking effects are dominative compared to the terrain-induced environmental heterogeneity downwind of the mountain. The isolated bell-shaped mountains tended to shift the track of the storm towards the left of storm motion; however, when the terrain was elongated the effect tended to be rightward. The terrain blocking effect also enhanced the supercells inflow. This allowed the central region of the storm to exhibit clouds with a greater density of hydrometeors than the NMTN control. Moreover, the enhanced inflow increased the areal extent of the supercells' precipitation, which strengthened the cold pool and enhanced the storm's updraft until becoming strong enough to undercut and weaken the storm considerably. Orographic blocking enhanced low-level vertical vorticity directly under the updraft when the storm approached the mountain. A modified NWS Tornado Detection Algorithm is used to investigate supercellular tornadogenesis; it is found that blocking effects are dominative and that elongating the terrain axis approximately parallel to the storm motion produces the strongest enhancement to tornadogenesis. Although the simulated cases with the highest mountains produced the most tornadic thunderstorms it is seen that increasing the terrain height alone is not sufficient to enhance tornadogenesis. Furthermore, an effective Froude number is developed to determine the amount of effective blocking that several terrain configurations exhibit in relation to both the mean winds and the storm relative winds, and although this effective Froude number does order the terrain geometries in an appropriate

manner, it alone is not sufficient to concretely determine which orientation is most likely to enhance tornadogenesis in supercell thunderstorms.

CHAPTER 1

Introduction

It is a common misperception that mountainous terrain always acts as a barrier preventing supercell thunderstorms (SC) and tornadoes (SCT) from crossing this terrain. However, several studies document cases in which SCs and tornadoes successfully survive and cross mountainous terrain (Bluestein, 2000; Bosart et. al., 2006; Homar, 2003; Schneider, 2009). The issue is complex, addressing not only how mountains weaken or disrupt convective storms, but also how they can intensify storm systems, and influence low-level wind fields and other environmental conditions that can lead to tornadogenesis.

Little research has been done regarding regional SCs climatology throughout the United States with respect to terrain; additionally, Bunkers (2006) notes there is no study of the regional distribution of supercells for the United States, although he notes a few areas of the US that have more frequent SCs (Bunkers, Hjelmfelt, & Smith, 2006; Bunkers et al., 2006). Despite that there has not been a climatology of SCs with respect to US terrain, based on a comparison of terrain elevation maps and tornado statistics (Figure 1) from the Storm Prediction Center in Norman, OK one can, anecdotally, attribute terrain with having some level of influencing on the intensity of tornadoes. Broyles and Crosbie (2004) provided evidence of smaller "tornado alleys" (Figure 2) across the US based on a climatological study of long track violent tornadoes from 1880 to 2003 which are generally associated with SCs (Bunkers, Hjelmfelt, & Smith, 2006). Again based on the locations of the enhanced regions of long track violent tornadoes; terrain exerts some level of influence on either the strength or path of these tornadoes.

When discussing localized severe weather the influence of terrain generally must be considered. Although terrain influences on synoptic and mesoscale systems have been widely

studied (e.g. Smith, 1979; Chen et. al. 2011; Lin, 2007; Lin et. al., 2006; Witcraft et. al., 2005) and little research on orographic influence on SCTs has been conducted. This lack of research could be due to the rarity of SCTs within mountainous environments, or the limitations of observations, such as radars and soundings in mountainous areas (Parker & Ahijevych, 2007).

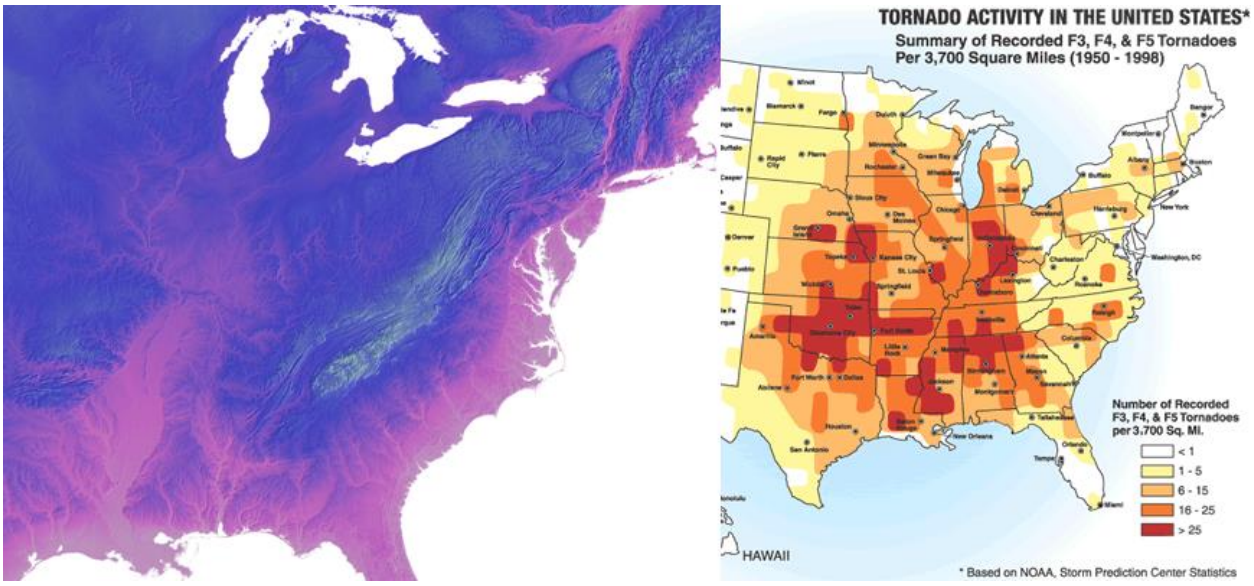

Figure 1. Comparison of Terrain Elevation Map (left) with Violent Tornado Activity in the United States from 1950 – 1998.

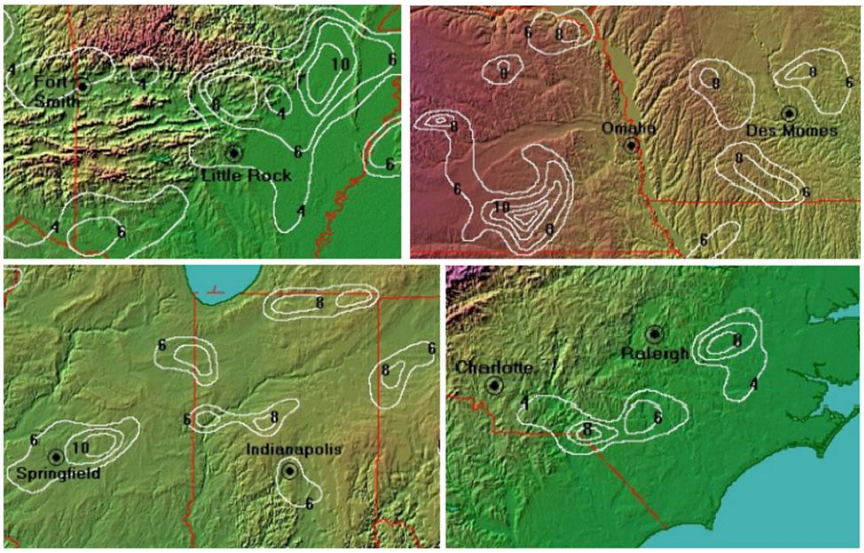

Figure 2. 1880-2003 F3-F5 Long Track Climatology of Violent Tornadoes.

Research on the orographic impact on SCTs has almost entirely focused on to case studies involving long track tornadoes over complex terrain (Bluestein, 2000; Bosart et al., 2006; Bunkers, Johnson et al., 2006; Gaffin & Parker, 2006). Although many (if not all) of these case studies call for numerical research to the authors knowledge only two numerical studies, i.e. Markowski and Dotzek (2011, denoted as MD11 hereafter) and Homar et al., (2003), have been done to determine the role that terrain has on supercell thunder storms and none have dealt with how terrain influences tornadoes. Nonetheless, future research is needed to determine the influences of terrain on SCs and SCTs, and whether it has a constructive or a destructive effect on low-level winds and other environmental aspects such as moisture, vertical shear, and localized temperature gradients.

Many studies on severe weather have considered large-scale synoptic conditions, but overlooked smaller mesoscale features (Bunkers, Johnson et al., 2006; Gaffin & Parker, 2006; Hocker & Basara, 2008b; Letkewicz & Parker, 2010). Additionally, many studies have focused on the effects that orography has on convective systems (Chu and Lin, 2000; Migietta and Buzzi, 2004; Chiao et. al., 2004; Frame and Markowski, 2006; Reeves and Lin, 2007). But evaluating topographic influences on SCs and SCTs, with a minimum of speculation, requires either high resolution simulations that can near fully determine the terrain influences at mesoscales or high resolution observations without missing data (Bosart et al., 2006). Since making complete high resolution observations is cost prohibitive at best in complex terrain; the study of SCs and SCTs in complex terrain is much better suited to high resolution simulations (grid spacing 500 m or smaller).

1.1 Significance of Study

The influence of terrain greatly complicates forecasting abilities for meteorologists through localized orographic effects (Rogers, 2006) and blocking radar observations by topographic obstructions. By studying the influence of terrain on SCTs, forecasters can gain a better understanding of the complex relationship and improve severe weather forecasting accuracy in mountainous regions (Hocker & Basara, 2008b; Dean and Imy, 2006).

As a specific example, during the 2011 New England Tornado Outbreak (2011NETO) ten tornado warnings were issued for the Massachusetts and southern New Hampshire area (Table 1). If all reported tornadoes are taken to be accurate; then four of these warnings were accurate. If only counting tornadoes reported by trained spotters or confirmed by damage surveying, then only two of the issued warnings were accurate. Additionally, the warning of the strongest tornado was issued thirteen minutes after it made contact with the ground and ended twelve minutes before the tornado dissipated. This is only a singular occurrence but it demonstrates that there is still much work to be done to increase lead times and greater accuracy when issuing tornado warnings.

The results of this research should allow forecasters to provide a better forecast when it is known that SCTs will intersect complex terrain.

Table 1

Summary of the ten tornado warnings issues during 2011NETO and actualized weather

Tornado Warning	Time Window (UTC)	Actualization
1	18:52-19:15	No Tornado, Large Hail Reported
2	19:28-20:00	No Tornado, Large Hail Reported
3	20:05-20:45	No Tornado, Large Hail Reported
4	20:30-21:15	Tornado Confirmed by Trained spotter at 20:32 Post analysis showed tornado was on the ground at 20:17-21:27 UTC, Rating EF-3, 39 mile track
5	21:01-21:45	No Tornado, Large Hail Reported
6	21:17-21:46	Unconfirmed tornado report by state trooper No post analysis confirmation or rating given
7	21:46-22:30	No Tornado, Large Hail Reported
8	22:07-23:00	4 Reported with 2 confirmed tornadoes by post analysis 22:32-22:40UTC, EF-1, 3.6 mile track 22:42-22.57UTC, EF-1, 1.3 mile track
9	22:57-00:00	Unconfirmed tornado reported No post analysis confirmation or rating given
10	23:12-00:00	No Tornado, Large Hail Reported

1.2 Research Objectives

This research intends to enhance the understanding of the orographic influence on SCs and SCTs by performing high resolution simulations (HRS) of SCTs in idealized terrain using the idealized sounding of Wiesman and Klemp (1982, 1984). Specifically we would like to determine:

1. What role, if any, underlying terrain can disrupt or augment rotational intensities of supercell thunderstorms, and
2. The relationship between topography and supercell thunderstorms.

To accomplish the above goals, this research will extendd the work of MD11 to conduct several idealized simulations using idealized bell-shaped mountains, initially round then elongated and rotated, with storms impinging at different locations.

CHAPTER 2

Literature Review

2.1 General Environment of Supercell Thunderstorms

Supercells usually develop in environments which are conditionally unstable and have directional wind shear at low-levels. A widely used parameter to estimate instability is Convectively Available Potential Energy (CAPE) in a flow with unidirectional shear. CAPE values larger than 2000 J Kg^{-1} are generally accepted as being conducive to SC development, although SCs have been observed with much lower CAPE values.

The significance of the relationship between CAPE and shear was quantified using idealized numerical simulations by Weismand and Klemp (1982, 1984). They investigated the effects of different combinations of CAPE and wind shear profiles. They found that multicellular thunderstorms formed when values of CAPE and shear were of low to moderate values, and SCs were formed in environments with high values of CAPE and shear. However, at intermediate values of CAPE and shear storms were likely to have characteristics of both SC and multicell storms. They defined the Bulk Richardson Number (1) as:

$$BRN = \frac{CAPE}{0.5(\overline{u^2} + \overline{v^2})} \quad (1)$$

where, $\overline{u^2}$ and $\overline{v^2}$ are the density weighted mean winds from 0-6km Above Ground Level (AGL) (Lin, 2007). Weismand and Klemp (1982, 1984) determined that the most favorable environments for SC development have BRN values between 15 and 45. Although these values were derived from idealized simulations, observations have generally agreed with these findings (Rasmussen and Wilhelmson, 1983).

Additionally, Observations of SCs environments have indicated that in addition to low-level shear being large, the shear vector also turns clockwise with height (Rasmussen and Wilhelmson, 1983; Barnes and Newton, 1986). Note that BRN does not take this directional shear into account.

An additional quantity used to account for the curvature of environmental winds is helicity. Helicity is defined as $H = \vec{V} \cdot \vec{\omega}$ where $\vec{V}$ is the environmental wind and $\vec{\omega}$ is the vorticity. Observations of long-lived rotating storms possess a large correlation between velocity and vorticity. Lilly (1986) suggested that SCs were long lived and predictable in nature because helicity suppresses the energy cascade into the inertial sub-range. Note that environmental helicity may not accurately reflect helicity entering the storm environment.

A quantity that accurately represents the helicity entering the storm environment is the Storm Relative Environmental Helicity (SREH) defined as (2):

$$SREH(\vec{c}) = \int_0^h (\vec{V} - \vec{c}) \cdot \vec{\omega} dz \tag{2}$$

where h is the depth of the storm inflow layer, $\vec{c}$ is the storm velocity, $\vec{V}$ and $\vec{\omega}$ are defined as in helicity. Note that storm motion must either be known or estimated to calculate SREH. Two rough threshold values for supercell development are $SREH \geq 150 m^2 s^{-2}$ and $SREH \geq 250 m^2 s^{-2}$ based on observations closest to the storm (Davies-Jones and Burgess, 1990) or based on numerical simulations (Droegemeier et al., 1993) respectively.

Droegemeier et al. (1993) initialized many numerical simulations by systematically varying the depth of the shear layer and hodograph curvature while keeping the shear vector constant. The results indicated that many storm types were possible for various environments

with the same values of CAPE and shear; this shows that mean shear does not precisely indicate the rotational characteristics of storm environments. They found SREH was a better predictor of storm rotation than BRN combined with helicity.

2.2 A Review of Supercell Thunderstorm Development

Supercell thunderstorms were first examined in detail during the 1960s, after Browning and Ludlam (1962) identified a particularly severe hailstorm that occurred near Wokingham, England, in July 1959. Browning and Donaldson (1963) later hypothesized that this severe storm, and a similar storm that occurred near Geary, Oklahoma, in May 1961 might constitute a new class of thunderstorms, which features steady three-dimensional circulations and long-lived updrafts that form in strongly sheared environments. Supercells were often observed to propagate to the right of the mean tropospheric winds and Browning (1965) hypothesized that this movement was due to the rotation of the storm's updraft. This model of quasi-steady, long-lived, rotating thunderstorms was a significant departure from the Thunderstorm Project (Byers and Braham 1949), in which thunderstorms were depicted as relatively short-lived phenomena, much like the model of ordinary (i.e., nonsupercellular) thunderstorms in use today.

Lemon and Doswell (1979) proposed a model of supercell thunderstorms which consisted of a primary rotating updraft that was fed by potentially warm and moist inflow, and two downdrafts consisting of potentially cool midlevel air which was chilled by the evaporation of precipitation into it (Figure 3). One downdraft, the forward flank downdraft (FFD), encompassed most of the main echo of the storm, whereas the rear flank downdraft (RFD) was located just to the rear of the updraft, near the hook echo and mesocyclone (Stout and Huff, 1953; Van Tassel, 1955; Fujita, 1958). The relatively cool downdraft air was separated from the warmer inflow air by the forward-flank and rear-flank gust fronts. It was noted that the FFD tended to produce a

weaker and more diffuse temperature gradient than did the RFD, which was generally colder. The illustration of two gust fronts wrapping into a mesocyclone resembles an extratropical cyclone qualitatively, although the dynamics are very different.

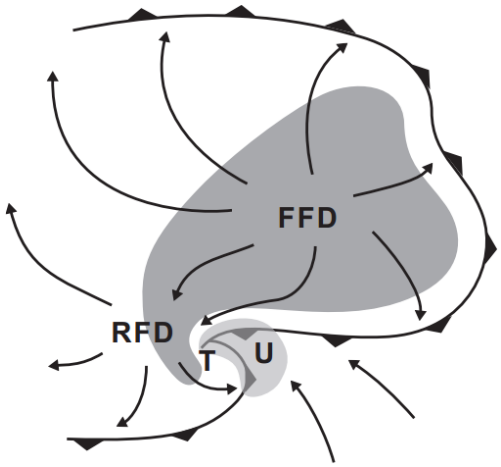

Figure 3. Lemon and Doswell's (1979) Supercell Conceptual Model

During the mid to late 1970s many cloud models were developed that could produce supercell simulations that closely matched many of the major observed properties of supercell thunderstorms. Using these cloud resolving models, Klemp and Wilhelmson (1978a), Wilhelmson and Klemp (1978) and Klemp and Wilhelmson (1978b) were able to simulate a supercell storm which split into a cyclonically-rotating right-moving supercell and an anticyclonically-rotating left-moving supercell. It was also found that the formation of precipitation-induced downdrafts was essential for storm splitting and that the commonality of right-moving supercells in the observational literature was not directly influenced by the Earth's rotation. It was determined that the Coriolis force indirectly favors the development of right-moving storms by influencing the synoptic-scale weather patterns and also through surface drag effects, both of which favor the development of wind profiles in which the hodograph rotates clockwise with height. This results in enhanced convergence on the right flank of right-moving

storms. These wind profiles also generate divergence on the left flanks of the storms, which is the area in which the updrafts of left-moving storms are often found.

Rotunno (1981) built upon these results using an analytical model of a supercell and concluded that tilting of the ambient horizontal vorticity present in a vertically sheared environment by an updraft results in a counter-rotating vortex pair at midlevels. Additionally, he showed that as this updraft intensified precipitation formed directly leading to a storm splitting downdraft.

As computing power has continued to increase, so has the scope of numerical simulations of supercells, investigators have examined the sensitivities of simulated supercells to changing wind profiles (e.g., Droegemeier et al. 1993; Brooks et al. 1994; McCaul and Weisman 2001), thermodynamic profiles (e.g.,Gilmore and Wicker 1998; McCaul and Cohen 2002; Kirkpatrick et al. 2007), and grid resolutions (e.g., Wicker and Wilhelmson 1995). From these added details it was determined that although many early observations of supercells revealed an approximately steady-state storm structure (e.g., Browning and Ludlam 1962; Browning 1964), cyclic behavior was demonstrated in supercell thunderstorm numerical simulations (e.g., Klemp and Rotunno, 1983; Wicker and Wilhelmson, 1995; Adlerman et al., 1999). The cyclical behavior was confirmed when later observational studies indicated that some supercell thunderstorms exhibited cyclic updraft and mesocyclone intensification and decay (e.g., Burgess et al., 1982; Beck et al., 2006). Adlerman and Droegemeier (2005) revealed a complicated relationship between environmental wind shear and the cyclic behavior of their simulated supercells (see their Fig. 21). Generally, they found that straighter hodographs tend to develop storms that cycled but did not fully occlude, while hodographs with more clockwise turning with height (e.g., circles and semicircles) tend to produce storms that cycled. As the magnitude of the

vertical wind shear was increased in these simulations, however, the modeled storms trended toward a non-cyclic, steady-state solution.

The overwhelming majority of previous simulations of supercell thunderstorms have been highly idealized, meaning that the simulations have generally been initialized with a single thermodynamic sounding and wind profile over a horizontally homogeneous domain. Often many factors are not included in a model or are turned off; this is generally done to reduce the number of parameters that have to be accounted for when investigating specific influences of the storm environment. The most common factor not included is terrain.

To the authors knowledge only two numerical studies have included the effect of terrain when simulating a supercell thunderstorm:

The first used the Mesoscale Model version 5.3, to simulate the environment of an August 1999 tornadic event in eastern Spain (Homar et. al., 2003). They did not attempt to simulate the tornado (the highest resolutions used in their simulations was 2 km), rather they determined an effective cap on the influence of terrain on the environment of this tornadic event. They determined that the influence of terrain features smaller than 10 km were responsible for a more intense supercell thunderstorm, whereas larger terrain features (20-50 km) was responsible for initiating the supercell thunderstorm. No physical mechanism was proposed for why small terrain features enhancing supercell circulation, but only stated such a link existed.

The second used the Bryan Cloud Model 1r13 (CM1) to simulate supercell thunderstorms that propagated past various two-dimensional and three-dimensional landforms of fixed height (Markowski and Dotzek, 2011). Their findings indicated that enhancements of convective inhibition and reductions of relative humidity correlating with depressed isentropic surfaces were most important in weakening updraft and mesocyclone strength. It was also noted that low-level

mesocyclones may be enhanced when interacting with terrain induced vertical vorticity anomaly despite reductions of relative humidity and enhancements of convective inhibitions. As this study is germane to ours it is covered in more detail in the next section.

2.3 Idealized Numerical Study of the Orographic Effects on Supercell Thunderstorms.

The specific focus of this study was the effect that ground relative winds have on modifying the environment of a propagating supercell thunderstorm. Specific to the three-dimensional simulations, the right moving storms are directed to intersect the point of maximum low-level vorticity identified in simulations with the same wind profile but no warm bubble was present to trigger convection.

MD11 used CM1r13 however this research uses CM1r16 because a bug was identified in CM1r15 and earlier releases that affects the calculation for horizontal gradients in simulations that have terrain and use a vertically stretched grid, this bug was corrected in CM1r16, a description of CM1r16 is presented in section 3.1 of this dissertation. The domain grid is stationary and is 100 x 250 x 18 km in *x, y, z* directions respectively with a horizontal grid spacing of 500 m and a stretched vertical grid spacing starting at 100m at the lowest model layer to 500 m at the top of the model domain. Additionally the domain is configured such that the lower and upper boundaries are free-slip and a Rayleigh damping layer occupies the uppermost 4km in order to prevent gravity wave reflection from the upper boundary.

Surface heat fluxes are turned off because the focus is on the interaction of mature storms with terrain and not the role of terrain in convective initiation. Due to the absence of surface heat fluxes, radiative forcing, and Coriolis force the model environment will remain steady during the simulation at least far from the influence of the terrain since airflow over the terrain will unavoidably evolve the model fields close to the terrain.

Figure 4 shows the sounding MD11 used to initialize the environment of the simulated storms, and the a graph comparing the relative humidity profile used in MD11 and the analytic relative humidity profile described by WK82. The sounding used is the WK82 sounding, with a reduced relative humidity profile achieved by reducing the exponent to 0.75, from 1.25, in the WK82 relative humidity equation (3),

$$RH = 1.0 - 0.75 \times \left(\frac{z_h}{z_t} \right)^{0.75} \tag{3}$$

where RH is the relative humidity, z_h is the height above ground, and z_t is the height of the tropopause (assumed to be 12 km), after which the relative humidity is set to a constant 0.25. Storms were initiated with an ellipsoidal warm bubble measuring a 10km horizontal radius and 1.5 km vertical radius with a maximum potential temperature perturbation of 2K. The bubble is centered 1.5km above the ground and 65-125km upstream of the terrain features so that the storms would pass over the terrain at approximately the second hour of simulation time.

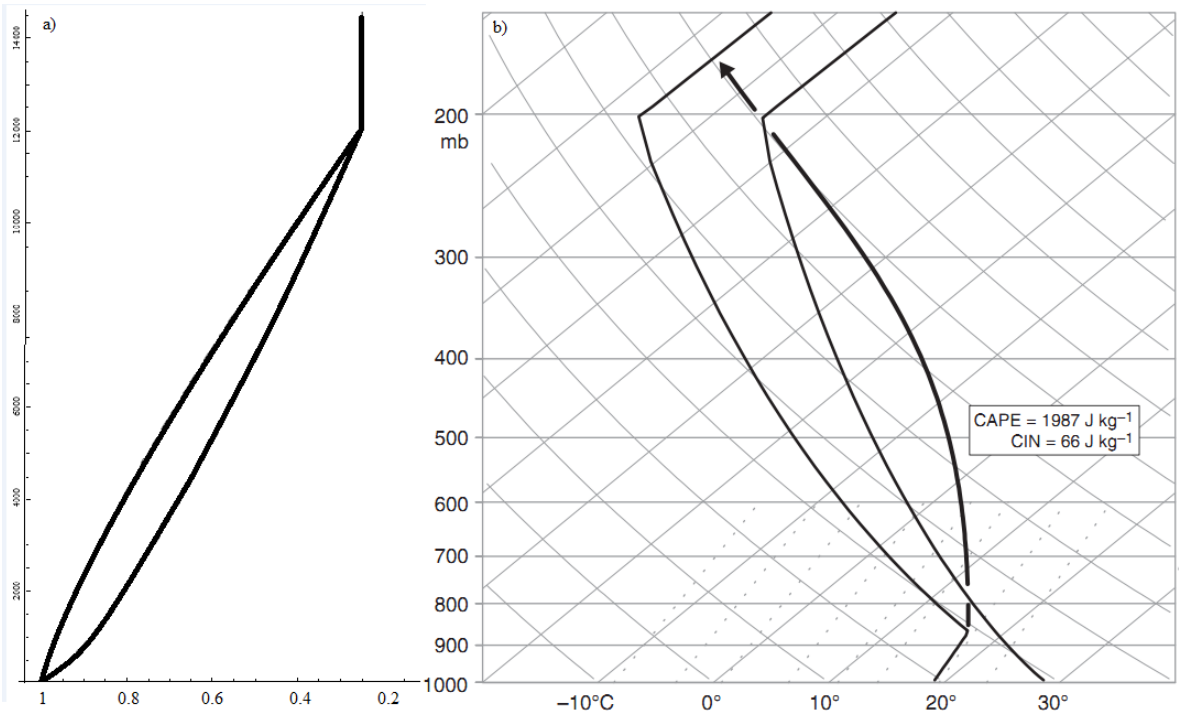

Figure 4. a) Comparison between the Relative Humidity Profile used by MD11 (left curve) and the WK82's analytic Relative Humidity profile (right curve), and b) The sounding MD11 used to initialize their simulations (Adapted from Markowski and Dotzek, 2011).

Adding a third dimension, the effects of terrain on the storm environment become further complicated by the addition of mesoscale vortices that can form in the lee of terrain obstacles. These vortices are believed to form baroclinically (Smolarkiewicz and Rotunno, 1989; Epifanio and Durran, 2002) rather than by the separation of a viscous boundary layer from an obstacle. The idea of a baroclinically generated vortex requires a stable stratified lower troposphere. These vortices are usually observed in environments where the Froude number $F_{rm} = U / N_{h0}$ is in the range of 0.1-0.5.

For the 3D simulations in MD11 the wind profile used is the one that presents the smallest degree of directional wind shear since this is the profile that produces the most prominent baroclinically generated vertical vorticity extrema in the lee of the isolated hill and

gap. Since the Froude number is larger than optimal for storm environments (around 1.3), there is a lack of well-defined vortices in the simulations. However, the flow is still able to produce distinct mesoscale vertical vorticity anomalies having a horizontal scale comparable to that of the mountain. The upstream wind profile favors cyclonic lee vorticity due to the hodograph curvature which causes the terrain-normal wind component to vary with height and this variation produced asymmetric lee vorticity anomaly in which the cyclonic member dominated. This cyclonic terrain-induced vorticity anomaly has a magnitude several times larger than that of the Coriolis parameter in mid-latitudes. The airflow over the mountain due to the higher Froude number also introduces horizontal heterogeneity in the CAPE, CIN, and SRH fields which are also seen in the 2-D simulations.

The terrain is a symmetric bell-shaped mountain (Equation (4)) and has a half-width of 10 km. Following the same concept as in the 2-D simulations, the terrain is configured so that the right moving supercell passes through the cyclonic vertical vorticity extremum induced by the terrain after 2 h of simulation time. The most significant cyclonic vorticity anomaly is centered 5 km southeast of the hilltop and exceeds 7.5×10^{-4} s^{-1}. Another maximum can be seen downstream but it is associated with a region of gravity wave-breaking and turbulence, which is not "targeted". When compared to the control case a gradual strengthening of the midlevel and the low-level updraft of the storm is seen as it encounters a region of upslope winds on the western slope of the hill followed by a weakening of the updrafts but a rapid spin-up of low-level vorticity as it passes over the primary cyclonic vorticity anomaly. The strengthening of the storm is due to decreasing CIN and increasing SRH on the upslope side of the hill. On the lee slope of the hill, CIN increases and SRH decreases which contributes to the weakening of the storm but since it encounters the terrain-induced cyclonic vertical vorticity maximum, a strengthening of

the low-level rotation is also seen. This shows that updrafts are more affected by thermodynamic conditions and/or vertical wind shear rather than environmental vertical vorticity perturbations. On the other hand low-level rotation responds quickly to these perturbations as seen by the weakening of the rotation as the storm moves east of the cyclonic vorticity anomaly.

Comparing this simulation to those made in 2-D flow (not shown) the weakening of the supercell is not as severe since in the 3-D simulation there is not a significant increase in CIN nor reduced relative humidity in the lee of the hill along its track south of the hill. Another simulation introduces a storm that passes north of the hill and over the anticyclonic vertical vorticity anomaly weakened noticeably upon encountering enhanced CIN and reduced relative humidity. The anticyclonic vorticity anomaly is smaller than its cyclonic counterpart so when this storm passes over this anomaly, it is unaffected by the environmental perturbation.

Regions of enhanced CIN, reduced relative humidity, and storm weakening in terms of updraft and mesocyclone strength are the regions where the isentropic surfaces were depressed relative to their far-field heights. By adding a third dimension, mesoscale vorticity anomalies can be generated. Although it is found that lee side vorticity anomalies affect the storm, it is hard to anticipate this since there are multiple factors on the lee generally lead to unfavorable conditions. The overall sense is that horizontal heterogeneity in the CIN, SRH, and relative humidity influences storms in more important ways than terrain-induced vorticity extrema. In these simulations, it appears that the influence of the terrain on the environmental air is what is most relevant.

MD11 should be regarded as a pilot study in the sense that everything is not yet explained then. Although the environmental heterogeneity could explain much of the behavior of the simulated storms, perturbations in environmental CAPE, CIN, SRH, etc. cannot explain

everything. MD11 identified multiple things not explored in this study; such as changes in the microphysical characteristics of the storm, depth of the outflow, gust front speed, precipitation, changes in terrain height and geometry, etc.; which could be important as well. For example, the depth of the outflow plays a major role in the maintenance of the cold-pool-driven convective storms, and even if dynamic vertical pressure gradients acting over a large fraction of the storm depth are crucial to the sustenance, supercell structure and evolution are not entirely independent of what goes on along the gust front (e.g., Ziegler et al., 2010).

MD11 stated that, additional work should be done on expanding the parameter space to different low-level stratifications, terrain amplitudes, and ground-relative wind speeds. Terrain can produce environmental heterogeneity in ways that the present simulations cannot replicate such as channeling of air by terrain which can lead to the superpositioning of air masses having different source regions, which could produce variations in CAPE and CIN that are more important than CAPE and CIN perturbations associated with terrain-generated gravity waves.

2.4 Tornadic Supercells over Complex Terrain: Case Studies

2.4.1 Tornadogenisis at Sistema Iherico, Eastern Spain-August 18th, 1999. An EF3 tornado occurred over the area of Sistema Iherico, Spain on August 18th, 1999. An area characterized by high terrain in excess of 2000 m is nicknamed “Sierra del Rayo” which means the lightning range. On this particular day, the area was in close proximity to an area of low pressure. As mentioned above, proximities to low pressure systems or frontal boundaries increase tornado potential. The low served to advect warm and moist air from the south, generate easterly winds, and increase shear; this combination of warmth, moisture, shear, and easterly winds primed the environment for tornadogenesis. In addition, mountain breezes aided upslope flow, contributing to rising air and updraft strength. The purpose of the study was to

investigate whether or not topographic features affect tornado development, and found that large scale terrain features at 20-50km, as well as small scale terrain features at 2-5km can enhance tornado potential (Homar, 2003).

2.4.2 Tornadogenesis at Divide, Colorado-July 12, 1996. On July 12, 1996, a F1 tornado with a path width of 50m, traveled 1.1 km through Divide, Colorado. This tornado occurred in the Rocky Mountains, a region characterized by rough topography and high elevations. Despite such complex topography, this tornado managed to form and traverse the terrain. A thorough investigation by Bluestein (2000) found the complex topography of the region may have enhanced upslope flow which helped augment updraft strength. Additionally, favorable southerly to south-easterly veering winds at the surface were present, enhancing wind shear conducive for tornado development. In this case the terrain, instead of inhibiting tornadogenesis, enhanced tornado potential by creating a favorable wind field to support tornado development (Bluestein, 2000).

2.4.3 Great Barrington, Massachusetts-May 29th, 1995. On May 29th, 1995 a significant tornado traversed rough terrain surrounding the Hudson Valley of New York and into Massachusetts. While reaching F3 strength, the tornado carved a 1 km wide path over a distance of 50 km causing three fatalities. An in-depth examination of this event showed a strong relationship between orographic features on supercell characteristics and tornadogenesis. On the day of the event the mesoscale environment, including wind shear and instability, was sufficient to support supercell development and tornadogenesis. Evaluation of the evolution of the storm over the terrain showed significant correlations between storm strength fluctuations in response to changes in terrain: the supercell strengthened over the Hudson Valley, became tornadic as it descended, downslope, east of the Hudson highlands, weakened as it ascended the Taconic

Range, and became tornadic again while descending into the Housatonic Valley. The assessment by Bosart (2006) illustrates the orography of the area facilitated tornado development by channeling warm, moist air through the valleys, strengthening wind shear profiles, and enhancing vorticity stretching as the storm descended to lower elevations on leeward ridges. This particular event illustrates that small-scale orographic features can overcome the large-scale inhibiting factors of terrain on storm development, and instead enhance severe potential. The question raised during this evaluation is whether a supercell thunderstorm must be strong enough to survive over complex terrain, or if the complex terrain instead enables the longevity and intensity of such storms (Bosart et al., 2006).

2.4.4 Three Tornado Events in the Southern Appalachian Mountain Region.

Schneider (2009) examined three documented cases of tornadoes across the southern Appalachians. In the three cases, Schneider suggested that local topography plays a role in enhancing tornadogenesis by: facilitating surface convergence, causing vorticity stretching as the storms moved from higher to lower terrain, channeling winds through valleys contributing to southerly and south-easterly backed winds, and enhancing updraft strength through upslope flow. All of the above strongly influence supercell strength and longevity by creating favorable conditions for each supercell to develop tornadic characteristics such as stronger rotation or stronger updrafts. Schneider (2009) specifically mentions that small-scale terrain features, such as features existing at the same spatial scale as supercells, are especially important in strengthening a supercell; small valleys or ridges that channel or back winds significantly increases wind shear and storm relative helicity (SRH) to create an atmosphere conducive to tornado development. Each of the three cases illustrate that regional topography might play an important role in tornado development.

The Tazewell, TN tornado occurred on April 26, 2007 and rated as an EF1 in intensity. The area was in close proximity to a boundary which aided in advecting warm, moist air from the south. Additionally, upslope flow created strong southerly winds, allowing for the backing of winds and strengthening of updrafts. As the supercell descended the lower elevations into the Tennessee Valley, it is suggested that vertical vorticity stretching ensued, resulting in tornadogenesis (Schneider, 2009). In this case, terrain features appeared to have aided in backing the winds, strengthening the updraft, and causing vorticity stretching.

The Big Stone Gap, VA was the location of an EF1 tornado that occurred on March 4, 2008. The surrounding mesoscale environment favored tornadic development with high shear and ample storm relative helicity along with prevailing easterly winds. The Powell River Valley, oriented southwest to northeast, played a role in backing the winds which enhanced low-level wind shear and storm relative helicity. This represented a possible example of a small-scale terrain feature acting as a positive influence on tornado development.

The third tornado event transpired in Kimball, TN on November 14, 2007. A long-track supercell traveled across most of Tennessee and produced an EF2 tornado in Marion County, where Kimball is located. The Sequatchie Valley, a topographic feature oriented southwest to northeast, backed surface winds to an easterly direction, and increased wind shear and storm relative helicity. As the supercell moved over this specific region, it rapidly developed a rotating updraft, mesocyclone, and eventually the EF2 tornado.

Schneider examined these three events within the Appalachian Mountains to gauge if terrain features impacted tornadogenesis. He suggested a possible relationship between terrain enhancements and tornadogenesis, but mentioned more in-depth studies should be carried out to find more conclusive evidence (Schneider, 2009).

CHAPTER 3

Orographic Effects on Supercell: Development and Structure, Intensity and Tracking

3.1 Model Selection and Description

Our simulations utilize the CM1r16 (Bryan and Fritsch, 2002) is a non-hydrostatic idealized numerical model designed to utilize high resolutions, particularly for severe local storms which contain deep moist convection. The governing equations that CM1 utilizes conserve mass and total energy, but they are not fully conserved in the model due to limitations in numerical integration. The CM1 introduced new equations for calculating gradients that better conserve mass and energy in simulations containing terrain and that employ stretched vertical coordinate. CM1 uses the Gal-Chen and Somerville (1975) terrain-following coordinates to map the model levels to the terrain while the model top is at constant height, and the governing equations are adapted from those described by Wicker and Skamarock (2002). The advection terms are discretized using fifth-order spatial finite difference and artificial diffusion may be applied both horizontally and vertically using separate coefficients. The sub-grid turbulence parameterization is similar to the parameterization of Deardorff (1980). CM1 has several options in microphysics parameterization schemes and the default scheme is the Morrison double-moment scheme (Morrison, 2005).

3.2 Model Configuration and Experimental Design

The domain is 300 × 100 × 18 km in the x, y, and z directions, respectively. In order to study the impacts of terrain on a storm, the grid is stationary, instead of moving with the storm; otherwise the path of the storm will be affected. The horizontal grid spacing is 500 m; the vertical grid spacing varies from 25 m in the lowest 500 m, to constant 500 m from 11 to 18 km (74 vertical levels total). The environments are horizontally homogeneous at the start of the

simulations except in cases where storms were initialized with a warm bubble, 2 K warmer than the environment, centered 46 km north and 35 km east of the southern and western domain boundary, respectively. The warm bubble was centered at 1.4 km above the lower boundary, was 1.4 km thick and had a horizontal radius of 10 km. Simulations were run for a period of 4 h.

Simulations with storms were initialized in a way that the supercell arrived near the terrains central point at approximately the 180 min of simulation time (i.e. the supercell would be quasi-steady when it interacted with the terrain). In addition, the location was chosen such that the supercell propagated as close to the peak of the terrain as possible.

The terrain used in this research is centered at 200 km from the eastern boundary and 50 km from the northern and southern boundaries and is a bell-shaped mountain. The bell-shaped mountain is defined by the following:

$$h(x,y) = \frac{h_m}{\left[1 + \left(\frac{x - x_0}{a}\right)^2 + \left(\frac{y - y_0}{b}\right)^2\right]^{3/2}} \tag{4}$$

where h_m is the mountain height, a and b are the mountain half-widths, and (x_0,y_0) is the center of the mountain. The half-width is a constant 10 km in both the x and y directions and the height is varied from flat terrain to 500 m, 1000 m, and 1500 m bell-shaped mountain. Keeping the half-width the same effectively increases the terrain blocking and lifting effect.

The lower boundary is free-slip and the upper boundary utilizes a Rayleigh damping layer (Durran and Klemp, 1983) in the uppermost 3 km of the model domain so that gravity waves generated by the terrain and convection are not reflected back into the domain. Lateral

boundaries are open and radiative (Durran and Klemp, 1983). Surface heat fluxes, atmospheric radiative heating, and the Coriolis force are set to zero for our simulations. The simulation uses the NASA-Goddard version of the Lin-Farley-Orville (LFO) microphysics parameterization scheme (Lin et al., 1983)

The environments of the simulated storms are initialized with a sounding very similar to the analytic sounding of Weisman and Klemp (1982, 1984 denoted as WK82 hereafter) (Figure 5) and a warm bubble as described above. Although it has been found that models initialized with the WK82 (standard) sounding resulted in a moist absolutely unstable layer when ascending over a relatively small hill (Bryan and Fritsch, 2000; Markowski and Dotzek, 2011); we believe that this was due to issues with the way previous models handled momentum and energy, as our model output did not indicate a moist absolutely unstable layer generated by the terrain.

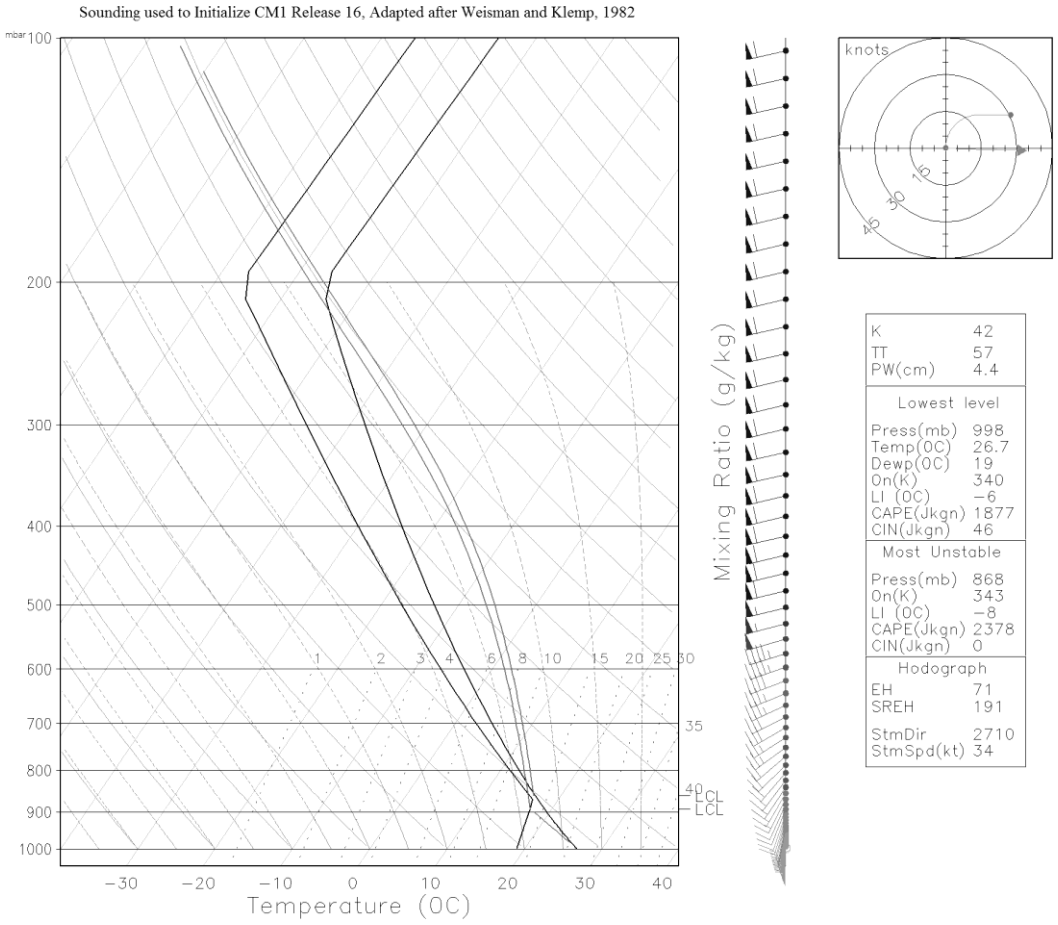

Figure 5. The sounding and wind profile used to initialize simulations in this study (Adapted after Weisman and Klemp, 1982). The hodograph can be seen in the upper right corner and several indices are indicated to the right of the wind profile. The black lines represent the dew point temperature and the temperature, left and right respectively. The grey lines represent the surface parcel ascent for the lowest level and the most unstable level, left and right respectively.

The sounding has a mixed layer convective available potential energy (MLCAPE) value of 1955 J kg^{-1} and a mixed layer convective inhibition (MLCIN) of 33 J kg^{-1}. The environmental wind profile is defined by the analytical quarter-circle hodograph described by WK82 (Figure 5). The WK82 wind profile has a bulk shear (0–6 km shear vector magnitude) of 32 m s^{-1} and storm-relative helicity (SRH) of 191 m^2s^{-2}. The *supercell composite parameter* (Thompson et

al., 2005 and 2007) of this wind profile is approximately 15. This is not surprising since the vertical moisture and wind profile for the WK82 was developed to simulate supercellular convection (although many of the included soundings in their analysis were tornadic). Moreover, the *significant tornado parameter* (STP) is greater than 2. Note that values of the STP greater than 1 are associated with the majority of tornadoes stronger than F2 while non-tornadic supercells are associated with STP values less than 1 (Thompson et al., 2005, 2007).

3.3 Environmental Simulation (Mountain Only – MTNO)

To investigate how the environment evolved with a mountain without the presence of a storm, simulations were performed with bell-shaped mountains of 500, 1000, and 1500 m heights. One method to measure the terrain blocking effect is the moist Froude number ($F_{w)}$ and is defined as $F_w = U/(N_w h)$ (e.g., see Lin (2007), Chen and Lin (2005), and Emanuel (1994)), where U is the basic wind, N_w is the unsaturated moist Brunt–Väisälä frequency, and h is the mountain height. Both the basic wind and the Brunt–Väisälä frequency are averaged over the depth of the mountain. Changing the terrain heights effectively varied the F_w to be 1.78, 0.89, and 0.59; for the above terrain heights respectively.

The model output for these MTNO simulations showed a general region of reduced MLCIN over and around the underlying terrain (mostly associated with a reduction in the distance from the surface to the Lifting Condensation Level LCL), however, as the simulation progresses, the greatest MLCIN reduction occurred just north-east of the mountain peak. Evidence of gravity waves modifying MLCAPE were present starting 90 min into the simulation as regions of alternating reductions in MLCAPE were seen radiating away from the terrain toward the east-north-east (Figure 6). Moreover, the control simulation output showed a general region of increased MLCAPE over and around the underlying terrain, with the greatest

MLCAPE increase occurring near the peak of the 500 m terrain. However, as the terrain height is increased above the LCL there is an associated reduction in the MLCAPE that evolves throughout the simulation to produce lower MLCAPE over the terrain peak (Figure 6). As with the MLCAPE field, evidence of gravity waves modifying MLCIN was present with alternating regions of increased/decreased MLCIN radiating away from the terrain toward the east-north-east.

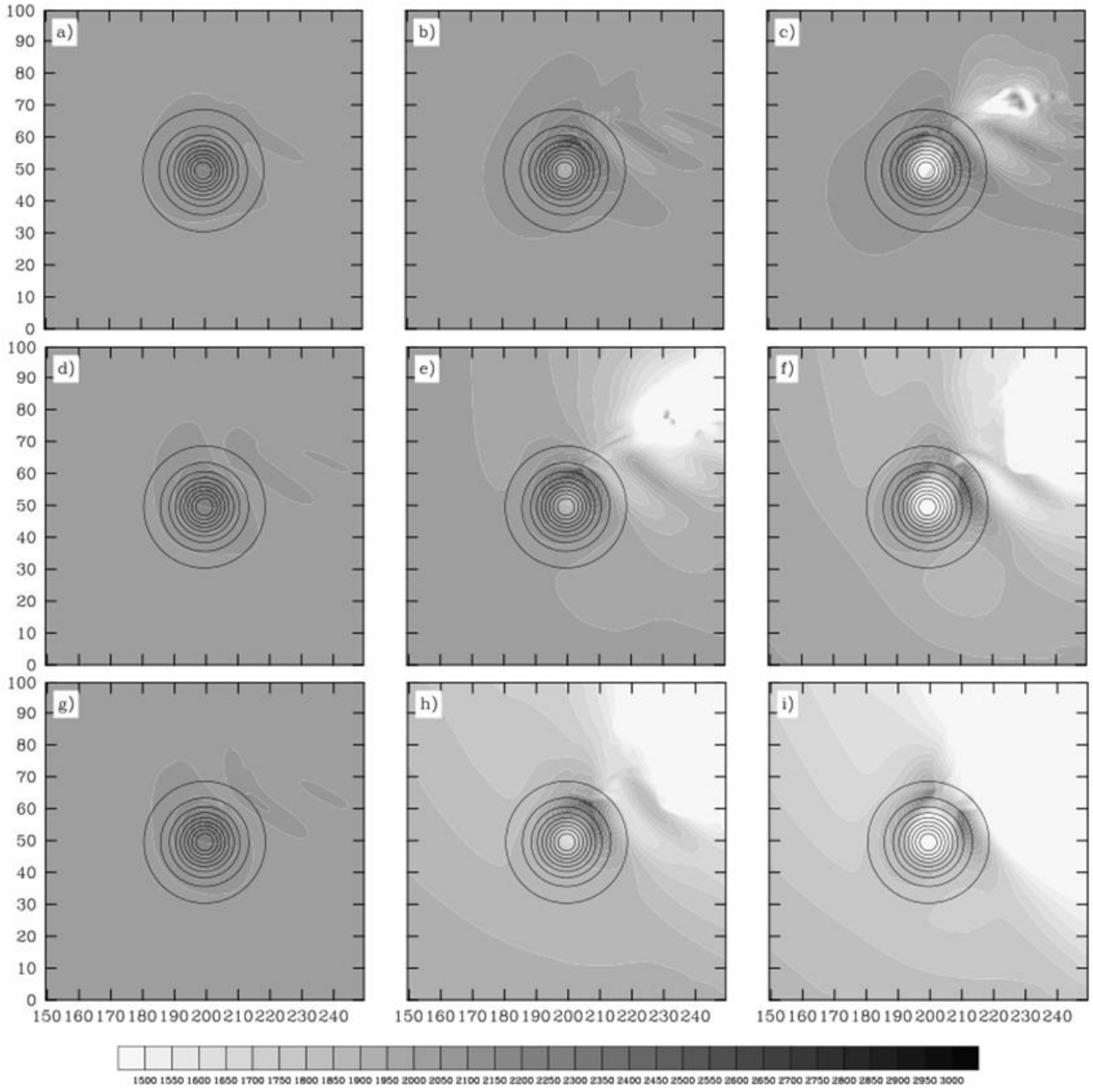

Figure 6. MLCAPE for simulations with the columns panels represent h_m = 500, 1000, and 1500 m (left to right); and the row panels represent different times at 60, 120, and 180 min. Note the region of depleted MLCAPE in c, e, f, h, and i are associated with storms triggered by terrain induced gravity waves. The contours represent the percent reduction in height; each contour from the peak represents a 10% reduction.

In simulations with higher mountains the modifications to MLCAPE/MLCIN were stronger, and in fact, supercellular convection was initiated by terrain induced environmental modifications (gravity waves) at approximately the 60 and 120 min for the 1500 and 1000 m simulations respectively. The location of the terrain induced supercell was approximately 40 km north-east of the terrain peak. It appears that this does not hinder our results as the cold pool did not significantly propagate over or around the mountain. Furthermore, the cold pool did not interact with that of the initialized storms until after our analysis is complete.

Further analysis of the low-level vorticity and wind field showed that the 1500 m terrain simulation is the only one that generated a closed pair of counter-rotating vortices (Figure 7). Although the maximum vertical vorticity generated by the 1500 m mountain was 0.013 s^{-1}, this was at the 60 min of the simulation and weakened by the 180 min. The vertical vorticity extrema, cyclonic and anticyclonic, is ±0.001 s^{-1} for the 500 m and ±0.0025 s^{-1} for the 1000 m mountain simulations.

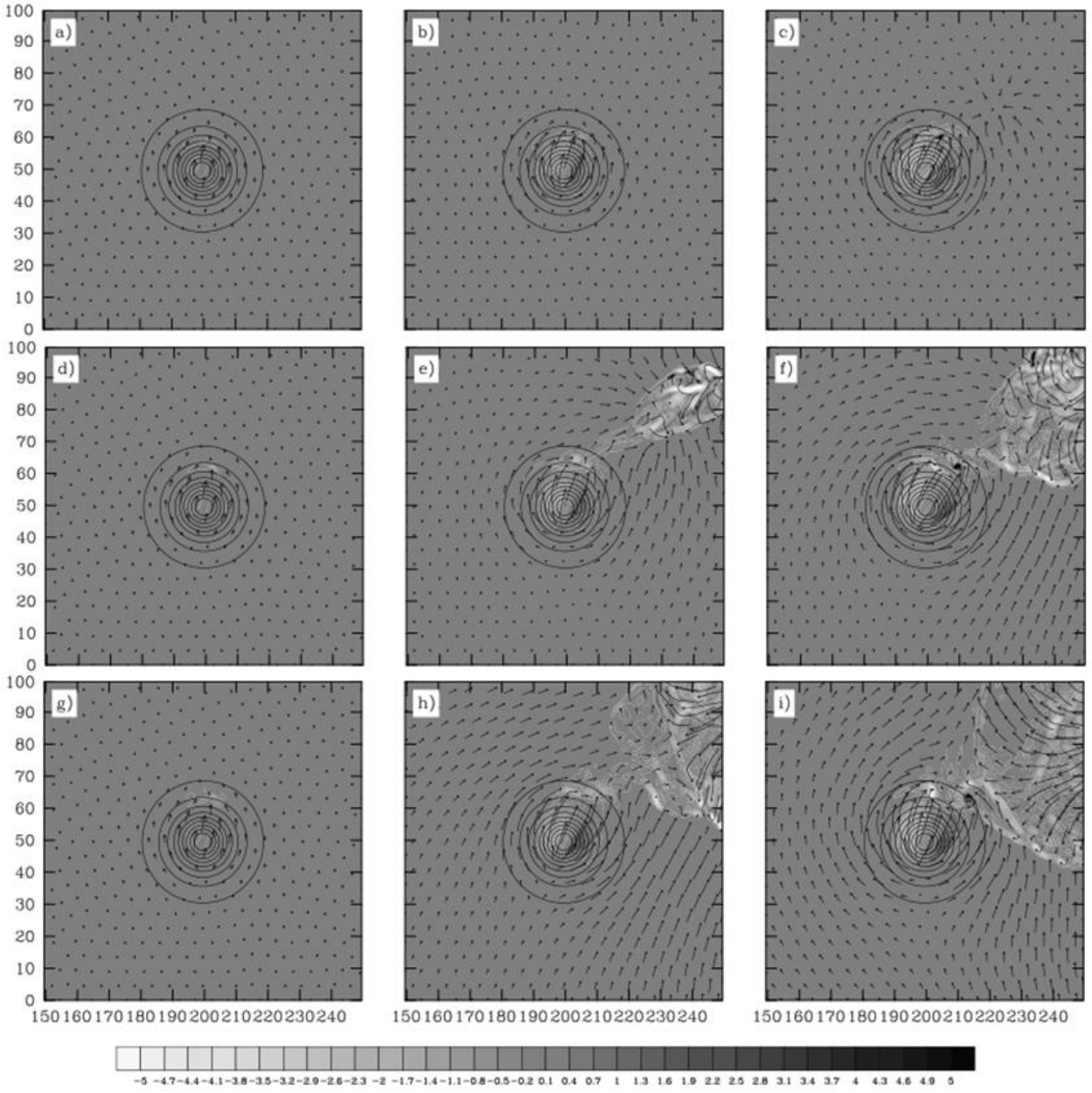

Figure 7. Low-level vorticity and horizontal wind vectors for simulations with column panels represent h_m = 500, 1000, and 1500 m (left to right); and the row panels represent different times 60, 120, and 180 min. Note the region of convergence associated with the outflow from the storms initiated to the north-east of the terrain. The 1500 m mountain was the only one that generated a closed pair of counter rotating vortices with vertical vorticities of 0.008 and -0.006 s^{-1}, respectively at the 180 min.

3.4 No Mountain Control Simulation (NMTN)

To establish a baseline of how CM1 simulates a supercell thunderstorm we performed a simulation without terrain. This simulation was initiated by the same warm bubble as those for the MTN (mountain) cases. This will also allow us to better isolate the effects of terrain.

The control simulation produced well-defined right-moving supercell thunderstorms with sustained midlevel, 5 km Above Ground Level (AGL), updrafts (downdrafts) exceeding 30 m s^{-1} (15 m s^{-1}) and low-level, 500 m AGL, updrafts (downdrafts) exceeding 5 m s^{-1} (10 m s^{-1}). Organization of midlevel rotation (vertical vorticity 0.003 s^{-1}) was incipient within 30 min of simulation time and was well organized by 45 min (with vertical vorticity 0.02 s^{-1}), see Figure 8. Midlevel cyclones were sustained throughout the end of the simulations and cyclic intensity is seen as indicated by the 1 km AGL updraft strength, see Figure 8; consistent with observations (Burgess et al. 1982; Beck et al. 2006) and previous numerical simulations (Klemp and Rotunno 1983; Wicker and Wilhelmson 1995). Simulated radar reflectivity gives a clear indication of the classic supercell structure at the 105th min Figure 9. It also shows that the midlevel rotation is aligned with the updraft, indicated by rotating winds aligned with the bounded weak echo region (BWER), which makes the storm more conducive to tornadogenesis. The control simulation vertical vorticities ranged from 0.02-0.05 s^{-1} 50 m AGL, from the end of 60 min. This storm propagates eastward at approximately 15 m s^{-1}, with small north to south variation in the location of the storm staying within approximately ±5 km north-south from the location of the warm bubble used to initiate convection.

The NMTN also had an anticyclonic left-moving storm that propagated out of the domain by 120 min.

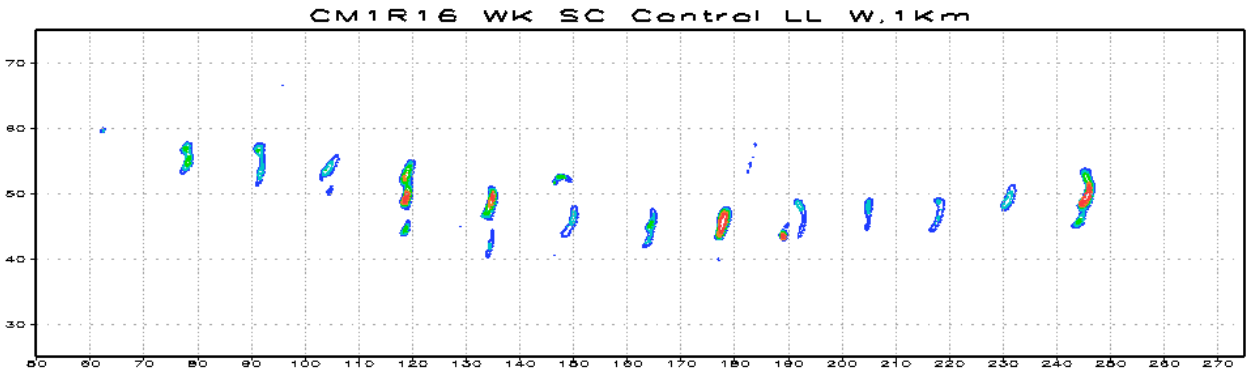

Figure 8. The cyclic nature of the simulated supercell thunderstorm can be seen in the strengthening and weakening of the 1km AGL updraft. Contours are blue, light blue, green, orange, and red representing the 10, 12.5, 15, 17.5, and 20 m s^{-1} wind speeds respectively.

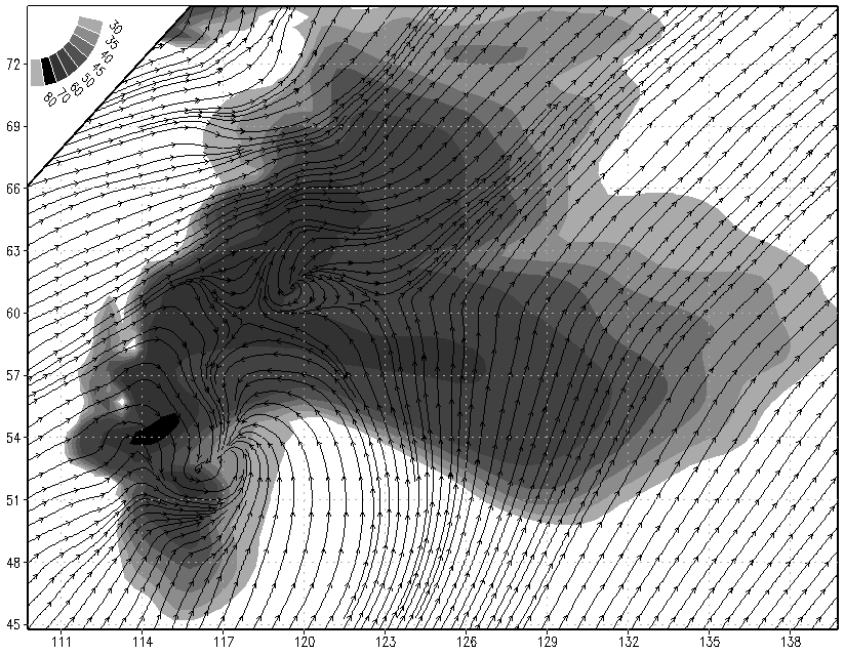

Figure 9. Reflectivity and wind stream-lines for the no-terrain control simulation (NMTN) at the 105 min. Note that the mid-level rotation is aligned with the BWER.

3.5 Mountain Simulations (MTN)

In the following we focus on the investigation of orographic effects on supercell thunderstorm; structure and development, intensity, and track.

3.5.1 Orographic Effects on Supercell Structure and Development. Overall the initial development of these supercells are quite similar for the NMTN and MTN simulations, the storms undergo more or less identical storm development during the first 60 mins of the simulation, and begin to exhibit the structure of the classical High Precipitation Supercell conceptual model (Lemon and Doswell, 1979). They remain structurally quite similar throughout the maturing phase, ~90 min, although there is increased rainfall area in the 1000 and 1500 m MTN cases, (M1000 and M1500 respectively). The structure of these storms diverged significantly by the 150 min.

A remarkable difference between the MTN cases and the NMTN case at the 150 min is the distribution of hydrometeors within the cloud. NMTN case has a distribution of cloud water and ice water that is approximately twice as large in horizontal extent as compared to the MTN simulations (Figure 10). The cloud size is partially attributable to the midlevel winds advecting the cloud and ice hydrometeors towards the east as the eastward winds are stronger in the NMTN case than in the MTN simulations, see Figure 10 and Figure 11. Furthermore, the cloud hydrometeor differences are also noticeable, which are related to the increased rainfall in MTN simulations reducing the overall amount of water available. The cloud that is indicated by reflectivity in the MTN simulations is accounted for as a mixture of snow and graupel hydrometeors. The decreased cloud region at the lower levels is also attributable to the updraft core being larger, stronger, and better organized in the MTN cases than that of the NMTN case.

The stronger updraft produced a larger over shooting top and allowed the anvil cloud to become deeper on the upwind side of the storm.

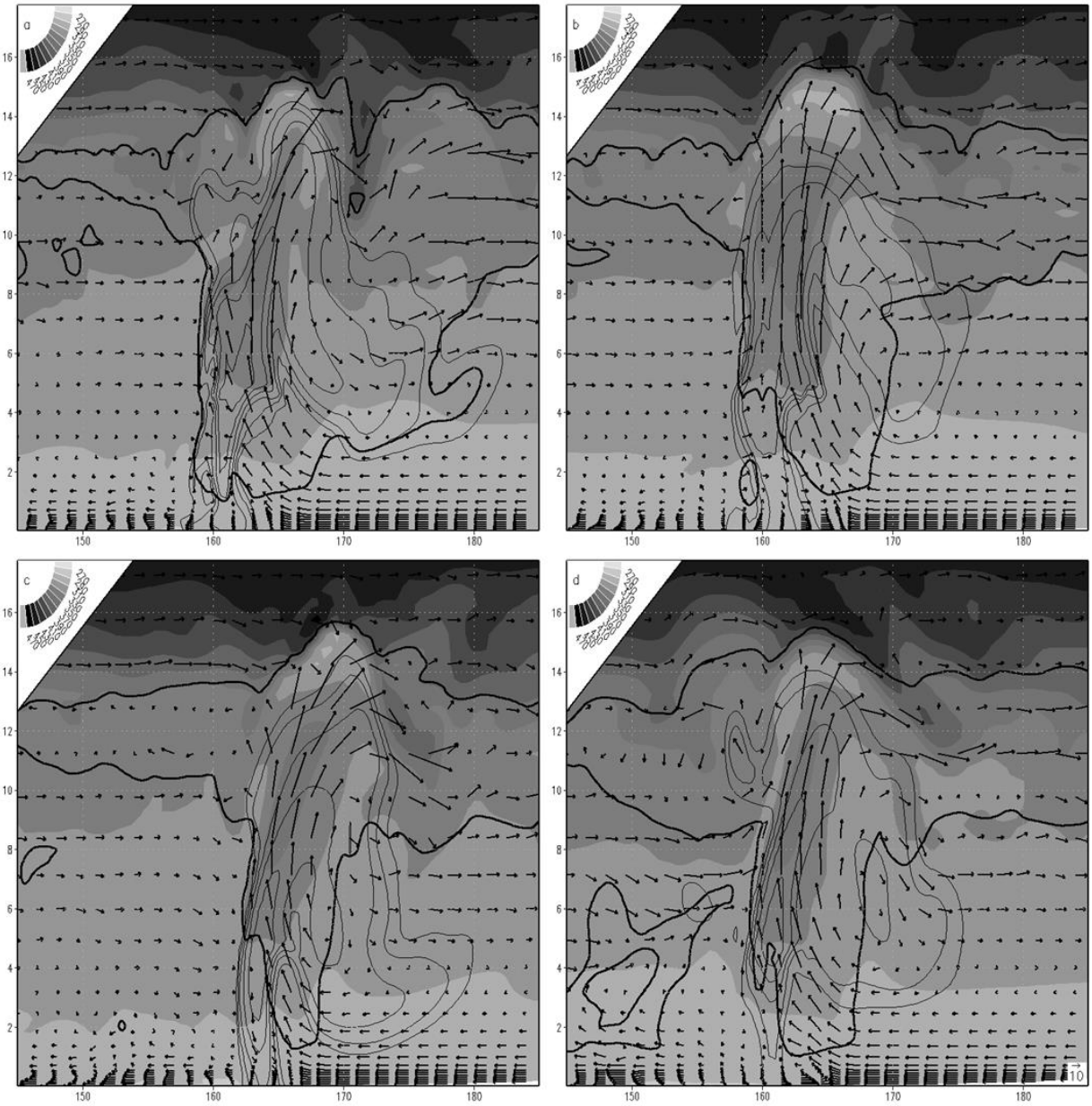

Figure 10. Zonal cross section of theta, reflectivity, cloud outline, and wind vectors, at the 150 min in cases NMTN, M500, M1000, and M1500 simulations a, b, c, and d respectively. Theta is shaded. Reflectivity values start at 50 dBZ and are contoured every 5 dBZ (thin contours). The cloud boundary is indicated by the 0.5 g kg^{-1} cloud water/ ice mixing ratio (bold contours). The reference vector is in the lower right corner of panel d and is the same for all panels. Cross section is along the direction of propagation (east-west) and is at the point of maximum UHW.

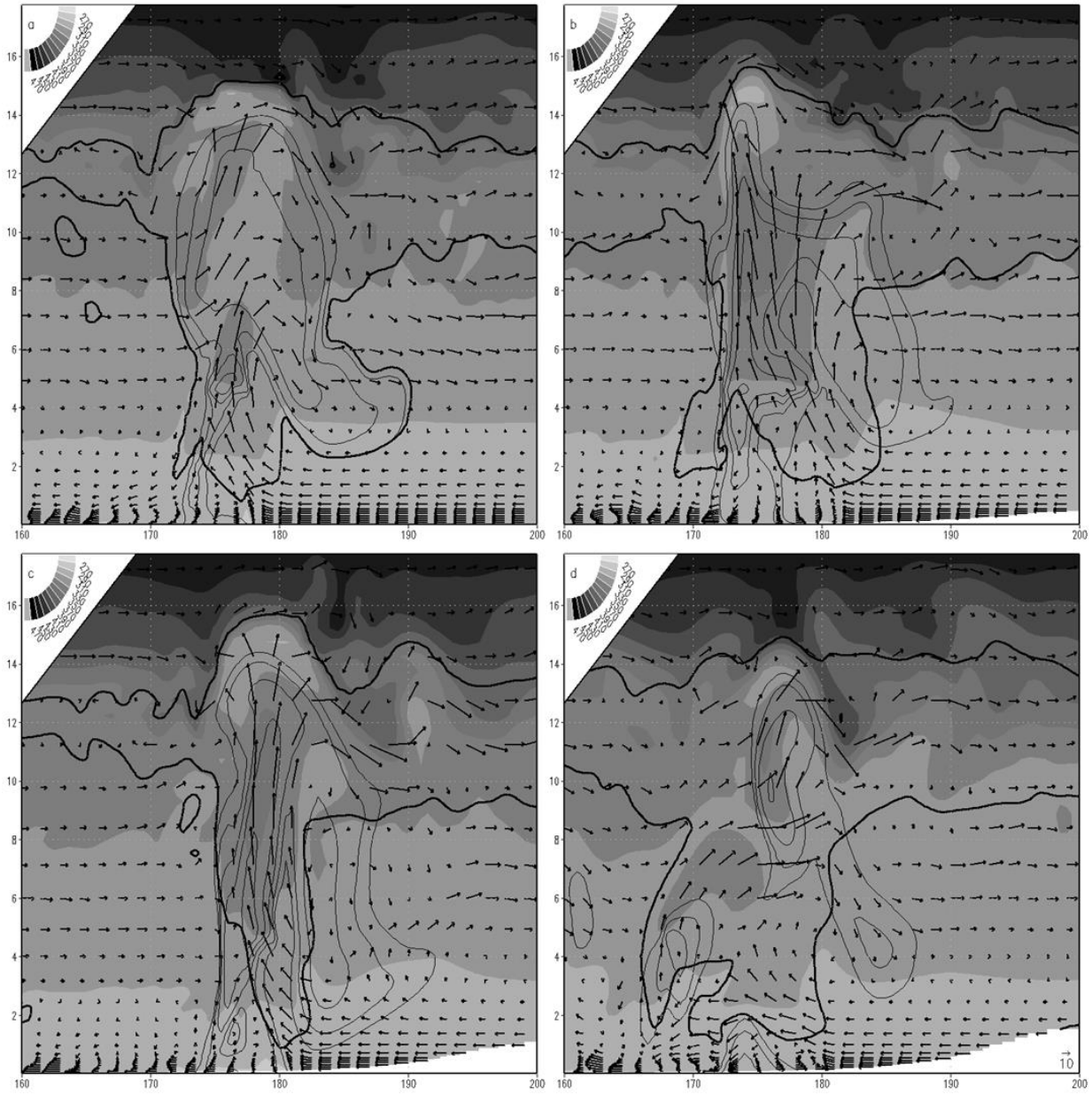

Figure 11. As in Figure 10 except for 165 min.

The hydrometeor densities in and around the main updraft region of MTN cases is higher than that of the NMTN case (not shown). The distribution of hydrometeors is primarily affected by the redirection of additional air into the storm modifying the storms structure; consistent with the findings of Curic and Janc (2012) in which they found that differential heating associated with terrain could alter the hydrometeor distribution.

The augmented air-flow into the supercell produced rain over a greater areal extent and a more continuous rainfall in the MTN cases. The rainfall area is also shifted towards the north in relation to the NMTN case. This is consistent with our findings that the track was shifted towards the north in MTN cases. The increased areal extent of rain allowed the cold pool to strengthen and intensify the storm until the gust front undercut the updraft which weakened the storms midlevel updraft considerably (Figure 10d and Figure 11d). The M1500 storm reorganized once it propagated away from the area where the gust front undercut the supercell.

The NMTN simulated storm developed a low pressure in the 6 to 10 km layer immediately east of the main updraft (Figure 10a), indicated by divergent winds associated with precipitation loading. As this low pressure strengthened (Figure 11a) winds from the main updraft were turned toward the east, until the main updraft was effectively split horizontally at approximately 8 km (Figure 12a). This shifted the cloud base to the east of the main updraft and reduced the rain rate as indicated by the reduction of reflectivity (Figure 10a-13a). Interestingly, the upper-level updraft intensified while the mid-level updraft weakened (Figure 12a and 10a).

The M500 simulated storm maintained its updraft size and strength more than those of the other simulations (Figure 10-13). The updraft became larger and stronger as the storm approached the mountain peak and the gust front converged with the winds which were diverted by the mountain. However, the larger updraft started to ingest air from its cold pool (Figure 10b and 13b) essentially offsetting the enhancement of the upslope winds coupled with the main updraft. This effectively produced a storm that varied less structurally throughout the time the storm was interacting with the terrain.

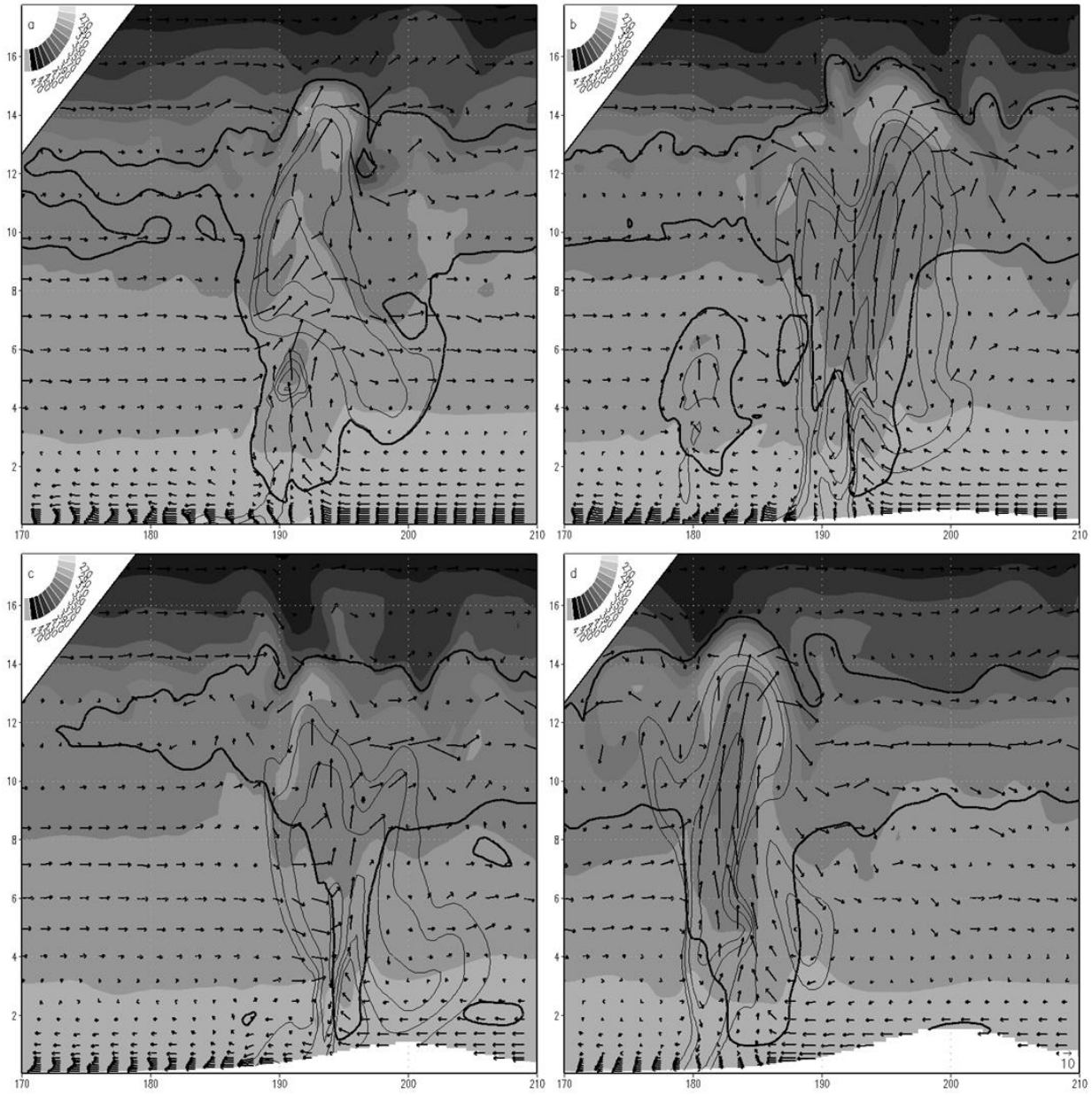

Figure 12. As in Figure 10 except for 180 min.

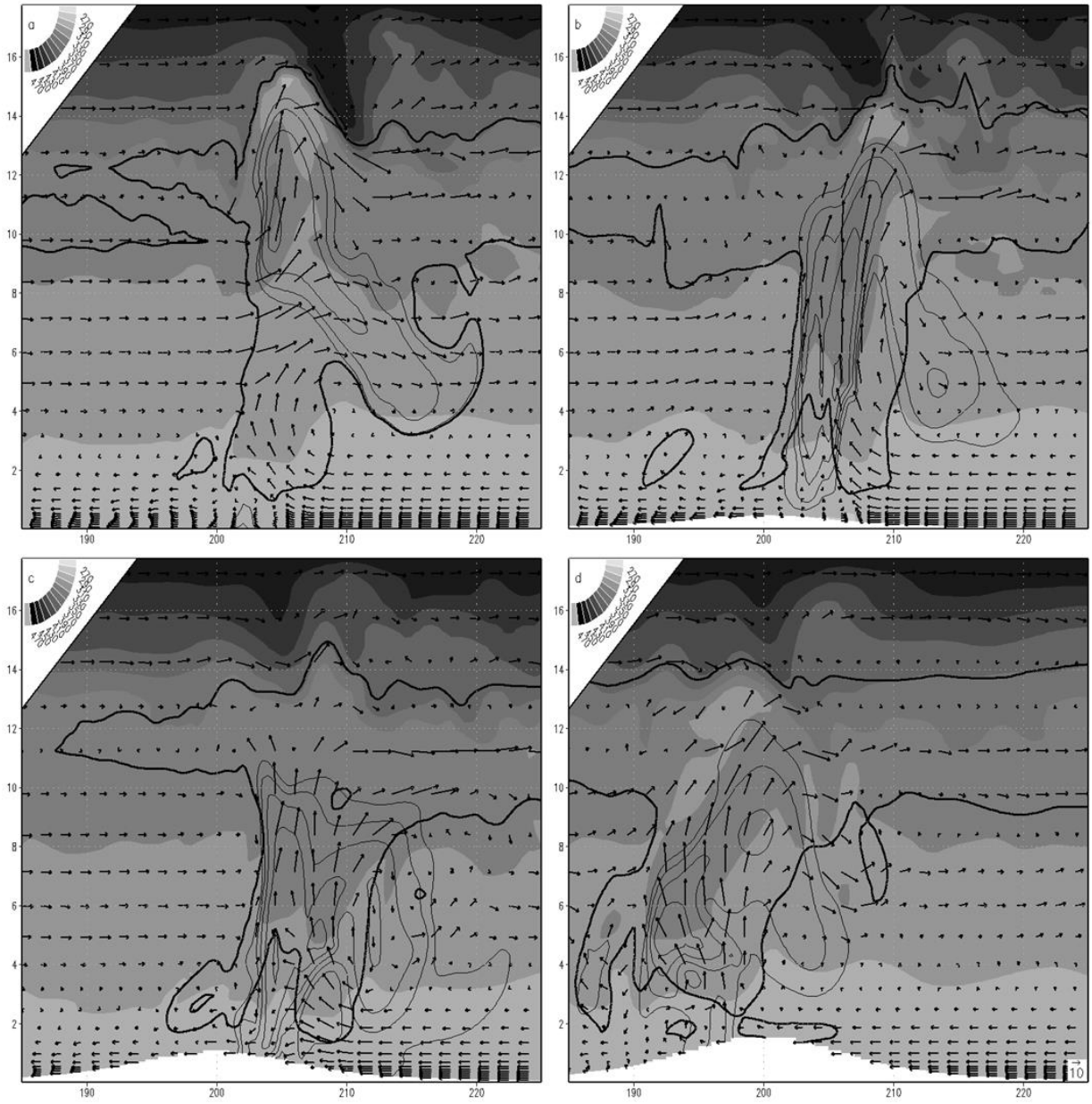

Figure 13. As in Figure 10 except for 195 min.

The M1000 simulated updraft intensified slightly and became more upright and the upwind part of the anvil cloud shallows as it approached the mountain (Figure 10c and 12c). However, as the storm propagated up the mountain the blocking effects on both the storm inflow and the cold pool weakened its updraft considerably (compare the low-level in-flow in Figure

11c and 13c). The blocking effect also reduced the storm's propagation speed which allowed the rear flank downdraft to interact with the storm's updraft, further weakening the storms main updraft (Figure 12c). Once the storm propagated to the lee side of the mountain, downslope winds coupled with the storms cold pool to enhance lifting of the lee side convergence region and the storms updraft became much larger (Figure 13c). The mid-level structure of the storm at the 195th min resembled that of the M500 simulation (Figure 13b and c). Once on the lee side of the mountain, the storm started to ingest cool dense air, which was associated with storms triggered further to the west of the mountain, and dissipated quickly after this time (not shown).

The propagation of the M1500 simulated storm was slowed when it started to interact with the terrain and thus it did not propagate past the mountain during the same time interval as that of the storms simulated in the NMTN or other mountain cases. The storm of M1500 was also slowed due to the reduction in the strength of the updraft associated with its ingestion of air from its cold pool and weakened considerably (Figure 10d and 13d). The ingesting of the cooler air from the cold pool also reduced the amount of precipitation, weakened the cold pool and allowed the storm to propagate out ahead of the gust front and re-intensified quite rapidly (Figure 12d). Once the supercell propagated further behind the mountain the inflow was blocked at low-levels and the inflow jet was essentially cut off from the storm (Figure 13d). Similar to the M1000 simulation the mid-level updraft widened considerably at 195th min. Once the storm propagated over the lee side convergence zone, the inflow becomes unblocked and the storm started to re-intensify up until the point that it started to ingest cold air from the terrain initiated storms, as mentioned in section 3.1 (not shown).

3.5.2 Orographic Effects on Supercell Intensity. Our intensity investigation will primarily focus on the strength of the updraft (downdraft) and the vorticity in the mesocyclone at

mid-levels (5 km AGL) and low-levels (500 m AGL); The impacts on tangential wind speed, how well the vortex is formed, and the strength of the gust front will also be discussed.

The supercell in all simulations exhibited cyclic intensification and decay, consistent with observations (Burgess et al. 1982; Beck et al. 2006) and previous numerical simulations (Klemp and Rotunno 1983; Wicker and Wilhelmson 1995). Although all simulations exhibited cyclic intensity the timing of the peak intensities was altered by the terrain such that it was shortened from approximately 75 min in the control case (NMTN) to 60 min in case with terrain (MTN). In both cases, there were three intensity peaks produced throughout the simulation. The change in the intensity cycle appears due to an increase in the storms inflow rather than the storms updraft coupling with the upslope winds of the terrain, as the second cycle peak is simulated before the upslope wind could become significant. After the second intensity peak of the NMTN and M500 simulations surface vorticity weaken whereas the M1000 and M1500 simulations intensify as the storms couple with upslope winds. On the lee side of the mountain the storms low-level updraft of MTN simulations weakens most notably in the M1500 simulation, while the M1000 and M1500 weaken considerably after the 210^{th} min as they encounter the area of reduced CAPE associated with the outflow of storms triggered on the lee side of the terrain. Although the first two intensity peaks in the MTN storms are stronger than that of NMTN storm the MTN storms are weaker at the third intensity peak.

Although a complete account of all minor variances of the terrain simulations from the NMTN simulation would be exhaustive and tedious, as they start after 60 min of simulation, very early from when the terrain effects become significant (nearly 100 km from the peak of the mountain). We look and the differences in the near surface vertical vorticities, the low and mid-

level updraft, and the speed of the gust front (a measure of the cold pool intensity) for the time interval from the 165 - 210 min.

At 165 min, the 1 km AGL updraft of the NTMN simulation was 15 m s^{-1} while the M500, M1000, and M1500 simulations were 9, 12, and 15 m s^{-1}, respectively (Table 2). The decrease in updraft velocity in the M500 and M1000 is most likely attributable to the hydrometeor density being higher in the main updraft resulting in precipitation loading. The downdraft for the M500 and M1000 simulations is stronger than the NMTN or M1500 simulations, 15 vs. 9 m s^{-1} respectively, as with the updrafts being lower the downdrafts are stronger due to the precipitation loading effect. At 5 km AGL the strongest updraft of the control simulation was 35 m s^{-1}, and is 30 m s^{-1} for all three terrain simulations. The downdrafts at this altitude are 15, 10, 15, and 5 m s^{-1} for the NMTN, M500, M1000, and M1500 cases, respectively. The speed of the gust front in the NMTN and M1000 simulations is 33 m s^{-1}, while the M500 and M1500 storms are 35 and 45 m s^{-1}, respectively.

At 180 min the M500 and NMTN simulations surface vorticity weakened by 0.011 and 0.004 s^{-1}, respectively. There was little change in the M1000 simulation vorticity and the M1500 simulation surface vorticity strengthened to 0.053 s^{-1} (Table 2). This increase in vorticity for the M1500 simulation was not due to the supercell coupling with the terrain induced vortex generated on the lee side of the mountain, as the storm's location is still relatively far from the location of the lee side vortex, ~30 km. The vorticity enhancement is due to stretching and terrain blocking effects physically redirecting air flow. The enhancement due to vorticity stretching is evident as the 1 km AGL updraft strength increases from 15 to 18 m s^{-1} during this time. Interestingly, the updraft of the M500 simulation increased in strength from 9 to 12 m s^{-1}, however in this simulation the surface vorticity decreased (Table 2), due to weaker coupling of

the storm's updraft with the upslope winds and reduced blocking effect not channeling the winds such that the vertical vorticity would be enhanced. At upper levels the updraft has strengthened for the M1000 and M1500 simulations by 10 and 5 m s^{-1} respectively and actually decreased for the M500 simulation. There was no change in the speed of the gust front for the NMTN or M1000 simulations; the gust fronts simulated in M500 and M1500 simulations were weakened by approximately 10 and 5 m s^{-1}, respectively.

Table 2

Selected Variables for intensity comparison from 165 - 210 min

Simulated Time	Case	w1km (m s^{-1})	w5km (m s^{-1})	Gust Front (m s^{-1})	Max θ' (K)	Surface Vertical Vorticity (s^{-1})
165 min	NMTN	15/-9	35/-15	33	-8	0.038
	M500	9/-15	35/-15	40	-7	0.031
	M1000	12/-15	30/-15	33	-8	0.025
	M1500	15/-9	30/-5	45	-8	0.038
180 min	NMTN	12/-15	35/-10	33	-11	0.034
	M500	12/-12	30/-20	30	-9	0.042
	M1000	12/-12	40/-10	33	-8	0.027
	M1500	18/-9	35/-15	40	-8	0.053
195 min	NMTN	9/-12	30/-15	30	-8	0.023
	M500	9/-15	30/-10	33	-8	0.023
	M1000	10/-10	30/-15	27	-8	0.031
	M1500	12/-10	30/-10	35	-8	0.035
210 min	NMTN	10/-10	30/-15	27	-8	0.027
	M500	10/-12	30/-10	33	-10	0.018
	M1000	10/-14	35/-15	24	-7	0.02
	M1500	8/-8	30/-10	30	-8	0.036

The increase or decrease in the updraft is attributable to two effects, the first and strongest contributor was the terrain blocking effect, which channeled air into the storm and coupled of the updrafts with the upslope winds. The turning of the winds increases the inflow wind speed from ~10 m s^{-1} for the NMNT storm to 16, 14, 17 m s^{-1} for the M500, M1000, and M1500 storms respectively, just as the storm is encountering the terrain. These together increase the precipitation rate (the rain coverage is increased in the M1000 and M1500 m simulations compared to that of NMTN and M500 simulations) (not shown) and strengthen the cold pool and intern the strength of the gust front. As expected higher terrain heights allowed the storms to generate consistently more rain.

The low-level vorticity is strongest and most organized in the M500 and M1500 simulations at the 180 min; the updraft is also aligned with the vertical vorticity (Figure 14). In addition to the vertical vorticity aligning with the updraft the down slope winds enhance the vertical vorticity by accelerating the horizontal winds on the northern section of the storm's updraft. It is possible that the M1000 simulation also experienced this enhancement of vertical vorticity by the downslope winds on the northern section of the storm's updraft; however the storms Rear Flank Downdraft proximity weakens the low-level updraft considerably (Figure 14).

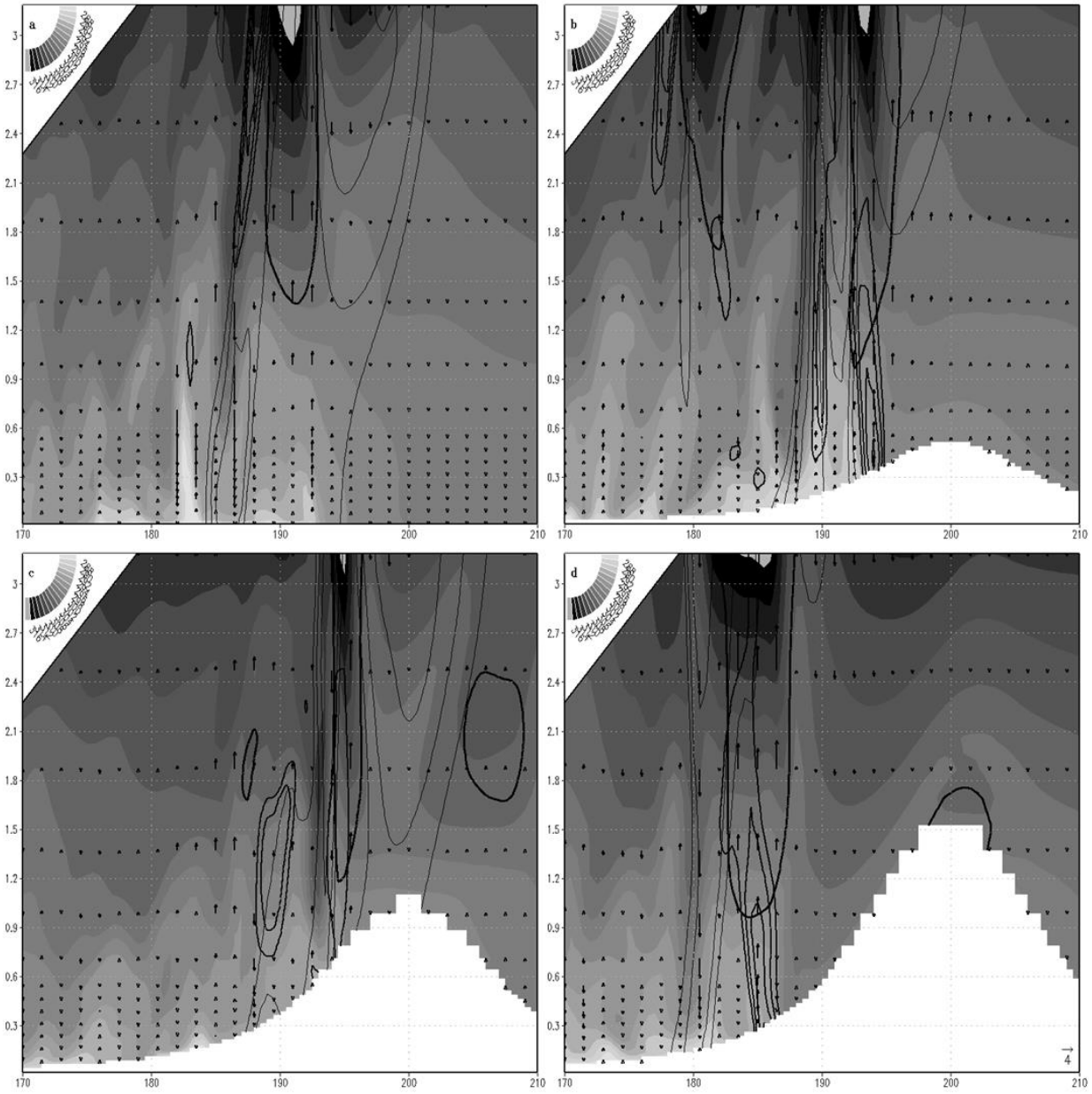

Figure 14. Close up vertical cross section along the east-west mountain ridge at the 180th min of simulation time. Theta, Reflectivity (starting at 50 dBZ, thin contours every 5 dBZ), Cloud outline (Thick contour), and Vertical Vorticity (Medium Contour, Levels are 0.01, 0.015, 0.02, 0.025 s^{-1})

3.5.3 Investigation of Methods for Tracking Supercell Thunderstorms and Orographic Effects.

A selection of parameters for determining the accurate location of a supercell thunderstorm is necessary for determining the track. First—assuming a supercell is present—we try to identify the location of the maximum updraft velocity which would yield a good track representative of the supercell's location. Although this provided a good starting point, the track was rather rough during the early part of the simulations when one would expect the simulations to be nearly identical (Figure 15a). Next, we identify the track using the classic identifier of a supercell the rotating updraft; this parameter is the updraft velocity, at 500 and 1000 m AGL, multiplied by the vertical vorticity at that level. This provided a smoother track than that identified by the maximum updraft alone. Using the classic supercell identifier we can conclude that the track is shifted towards the north in simulations with increasing mountain height.

We continue our investigation along these lines, and use the location of maximum updraft helicity (UH) to determine the supercells location, UH is a new parameter that has recently been used to identify the areas where convective storms are more likely to occur (Kain et al. 2008). UH has proved useful in its ability to detect areas more likely to exhibit convection in model output (Sobash et al. 2008). Although the UH did indicate that a storm was in the approximate vicinity of the supercell, the identified track was rather sporadic and produced quite an erratic track, this ruled out the usage UH alone as a supercell tracking method. The storm track was initially smooth during the storm's development phase; however the track became erratic throughout the rest of the simulation (not shown).

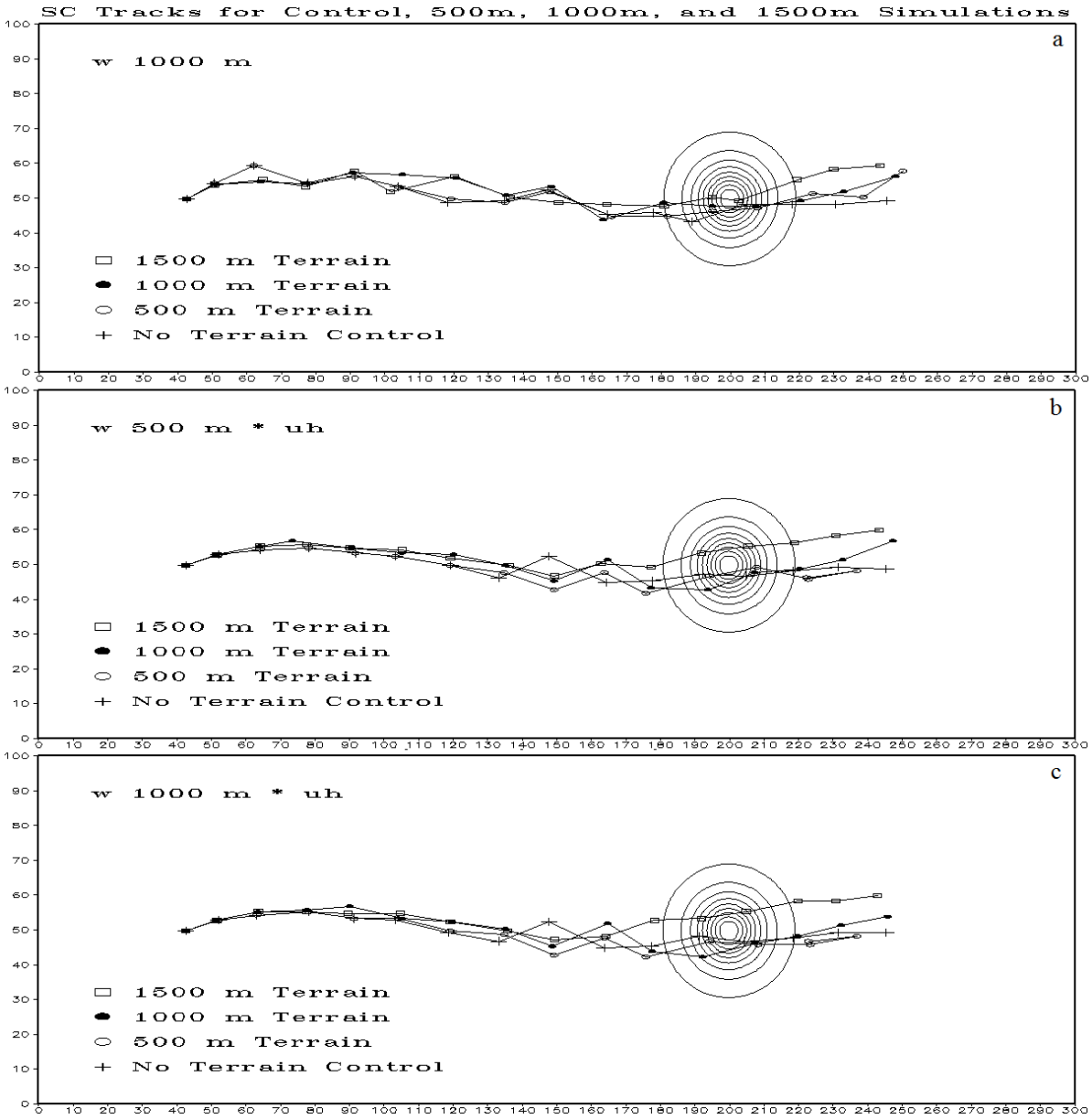

Figure 15. Tracks of supercell thunderstorms as identified by (a) 1000 m AGL Updraft strength (b) Updraft Helicity (UH) multiplied by vertical velocity at 500 m AGL (c) Updraft Helicity multiplied by vertical velocity (UHW) 1000 m AGL. The contours represent the normalized terrain height.

The next parameter used to identify the supercell's track was the maximum UH multiplied by the updraft velocity (UHW), which makes the track smoother than that identified by UH. The storm location was identified by tracing the maximum UHW. Again, we used the updraft velocities at 500 and 1000 m AGL. UHW noticeably improved the track and we can say that as the Froude Number decreases the supercell track is shifted towards the north, particularly at lower levels. The combination of the updraft with the updraft helicity produced a smooth track that was free of significant jumps and was more consistent at the two heights used to identify the supercells track.

Of the parameters used to identify the track of a supercell our UHW parameter yielded the best track; both based on smoothness and consistency (between different levels). Following closely after the UHW, the updraft strength produced the smoothest track as long as supercells are known to exist. The classic definition of a rotating updraft produced good results in track identification it produced jumps that were uncharacteristic of storm propagation. Interestingly the updraft helicity parameter yielded the poorest track identification with erratic track identification just after the initial strengthening phase.

3.6 Concluding Remarks

The effects of idealized, bell-shaped mountains on supercell thunderstorms were investigated in this study. The mountains produced gravity waves that modified the downwind environment by producing alternating reductions and increases in the amounts of moisture, MLCAPE, and MLCIN. The simulations with higher mountains, such as mountain heights of 1000 m (M1000) and 1500 m (M1500), produced gravity waves that had enough vertical motion to initiate convection near the 120 and 60 min respectively. Cold outflow from these storms reached the lee side at approximately the 225 and 180 min for the M1000 and M1500

simulations, respectively. Although these storms produced large environmental modifications our analysis was focused before these effects could influence the investigated supercells.

Several combinations of variables were used to create parameters for the identification of a supercell's location. Although the updraft helicity (UH) indicated the general vicinity of the supercell the identified track that was rather erratic. Other parameters that were used based on the characteristics of supercells yielded smoother tracks; however the maximum UHW (UH multiplied by the updraft velocity) produced the smoothest tracks and tracks that were the most similar far from the mountain where the terrain effects are minimal. Using the maximum UHW we identified that increasing the mountain height shifted the tracks of supercells towards the north.

The intensity of supercells was cyclic in all simulations; however the period between intensity peaks was reduced in mountain (MTN) cases as compared to the no mountain (NMTN) case. The intensity, structure and development of the storms were mainly a result of the mountain directing an increased amount of environmental air into the storms inflow. This created differences in the distributions of hydrometeors and increased the rainfall areal extent. This allowed the cold pool to be stronger in the MTN simulations, most notably when the cold pool undercut the M1500 storm.

Airflow was also modified such that vorticity was generated and/or intensified when approaching the mountain peak. The near surface rotation of the M500 (F_w = 1.78) storm intensified as it approached the mountain peak. The M1000 (F_w = 0.89) storms propagation speed was reduced as it crossed the terrain, which allowed the storm's rear flank downdraft to run into the storms low-level updraft and reduced the near surface vorticity greatly. The storm weakening as it approaches the terrain is also attributable to the terrain inducing modifications in

the storms life cycle. The M1500 (F_w = 0.59) storm experienced a greater reduction storm motion, however, its' rear flank downdraft was farther away from its updraft and its intensity was not affected in the same manner as M1000. The M1500 storm propagated around to the north of the mountain peak and its cold pool worked in conjunction with the terrain to block the storm's inflow and causing the storm to weaken considerably until it propagated into the lee side convergence region.

Although these simulations did not produce tornadic supercells as the grid spacing was too coarse to reproduce such systems, model output noted (in CM1's log files) several instances throughout the MTN simulations where vertical vorticity was greater than 0.1 s^{-1} at the lowest model level (12.5 m). We believe that tornadogenesis could occur if the simulations were run at higher resolutions.

We have shown that blocking effects may direct additional air into the storms inflow and enhance low-level vorticity along the gust front and that these blocking effects are far more important that the than the environmental modifications, especially since we observed these differences before the storm even interacted with the environmental modifications on the lee side of the mountain. The direction of additional moist air into the storm is particularly of interest to now/forecasting because this increases the precipitation amount and was observed far from the mountain and could increase the likelihood of flash flooding. The M1000 and M1500 simulations initiated supercellular convection that reduced the MLCAPE and increased the MLCIN far more than the gravity waves excited by the mountain and indeed when the simulated storms propagated into this region they quickly dissipated.

Areas where this study could be extended in the future are to vary the arrival time of the storm to investigate the terrain effects on developing or mature storms. Additionally, the track

and/or terrain configuration could be modified to test the robustness of our conclusion that the terrain blocking effects are more important that the environmental modifications. This area is still very much unexplored and additional research is needed.

CHAPTER 4

Effects of Orographic Geometry on Supercell Thunderstorms

4.1 Model Configuration and Experiment Design

The model configuration is as in Section 3.2 of this dissertation, except with the following modifications. The bell shaped mountain is elongated by extending the north-south axis of the terrain. Then the terrain is rotated to investigate the varying blocking effects. The terrain is rotated as follows. Starting with the general form of the function for the bell shaped mountain with center located at (x_0, y_0),

$$\frac{h_m}{\left[1+\left(\frac{x-x_0}{a}\right)^2+\left(\frac{y-y_0}{b}\right)^2\right]^{3/2}} \tag{5}$$

If we wish to rotate this mountain by an arbitrary angle θ about the peak of the terrain we first start with applying the rotation operator to the variable vector minus the vector pointing from the origin to the peak of the terrain in the non-rotated frame of reference (this is to keep track of the peak location during the rotation, i.e. so the peak will not move) (6),

$$\begin{bmatrix}\cos(\theta) & -\sin(\theta)\\ \sin(\theta) & \cos(\theta)\end{bmatrix} \times \begin{bmatrix}x-x_0\\ y-y_0\end{bmatrix} \tag{6}$$

The result of applying the rotation operator shows how to modify the non-rotated coordinates to equal the rotated coordinates, denoted by the subscript 1 in equation (7),

$$\begin{bmatrix}\cos(\theta)\cdot(x-x_0)-\sin(\theta)\cdot(y-y_0)\\ \sin(\theta)\cdot(x-x_0)+\cos(\theta)\cdot(y-y_0)\end{bmatrix} = \begin{bmatrix}x_1\\ y_1\end{bmatrix} \tag{7}$$

Now substituting the resultant coordinates from the rotated space into the general formula for a bell shaped mountain yields the formula for a rotated mountain in our non-rotated, (x_0, y_0), coordinate system (8).

$$\frac{h_m}{\left[1+\left(\frac{\cos(\theta)\cdot(x-x_0)-\sin(\theta)\cdot(y-y_0)}{a}\right)^2+\left(\frac{\sin(\theta)\cdot(x-x_0)+\cos(\theta)\cdot(y-y_0)}{b}\right)^2\right]^{3/2}} \quad (8)$$

The elongated bell shaped mountains have semi-major half widths that are twice the length of the semi-minor half widths, and are 20 km and 10 km respectively (Figure 16a, 16b). The rotated terrain is 45 degrees toward the west then toward the east (Figure 16c, 16d). Analysis will be conducted similarly to the preliminary results except with the addition of varying the impinging location. The extension of this work would add to the robustness of the preliminary results and further aid in understanding how various terrain configurations/orientations affect supercell thunderstorms.

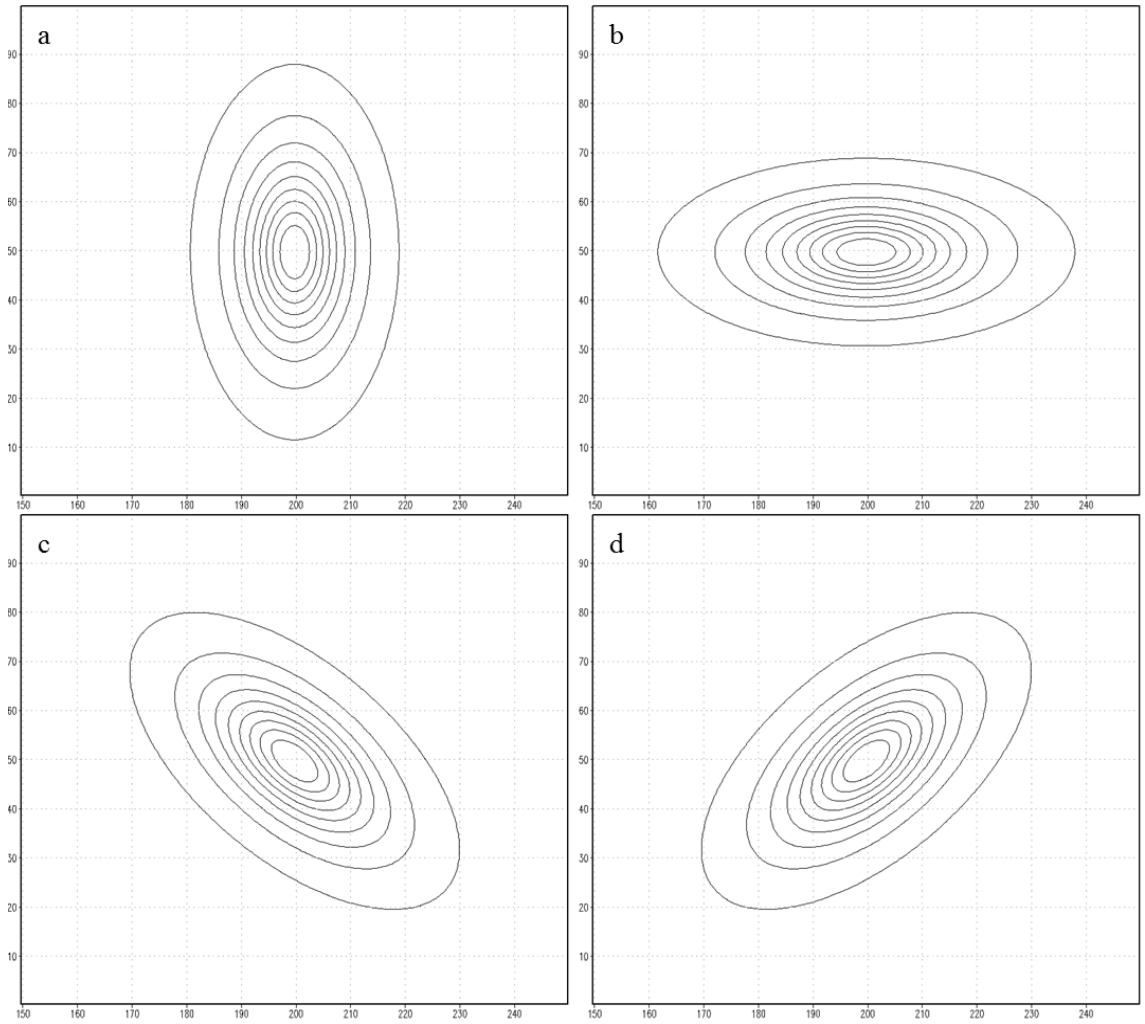

Figure 16. The four configurations of the elongated bell shaped mountains. a) 2B, b) 2A, c) RM45, and d) RP45. Each configuration has three mountain heights which are 500, 1000, and 1500 m.

4.2 Method for Tornado or Tornadogenesis Evaluation

In order to declare a storm tornadic we must develop a method for declaring what exactly we shall call a tornado. We will determine if a storm is tornadic in a manner quite similar to the tornado detection algorithm that is used by the National Weather Service to detect tornado signatures in radar observations. The tornado detection algorithm is modified and our method for tornado declaration is as follows:

1. The vortex at the lowest model level (LML, 12.5 m AGL) is closed and the cross vortex shear is greater than 25 m s^{-1} at the LML and the vortex has depth of at least 1.5 km

or

2. The vortex at the LML is closed, the vortex has a depth of at least 1.5 km and the cross vortex shear is greater than 36 m s^{-1} anywhere in the vortex.

Any storm that meets these qualifications we shall deem as a tornadic supercell for our investigation. Figure 17 shows an example of the difference between a closed vortex that comes from a simulation that meet criteria 1 and another simulation that meets everything in criteria 1 except for having a closed vortex. If we assume that a vortex requires at least 4 grid points to be adequately resolved then the minimum vorticity that could meet either of these requirements is 0.0225 s^{-1} for these simulations.

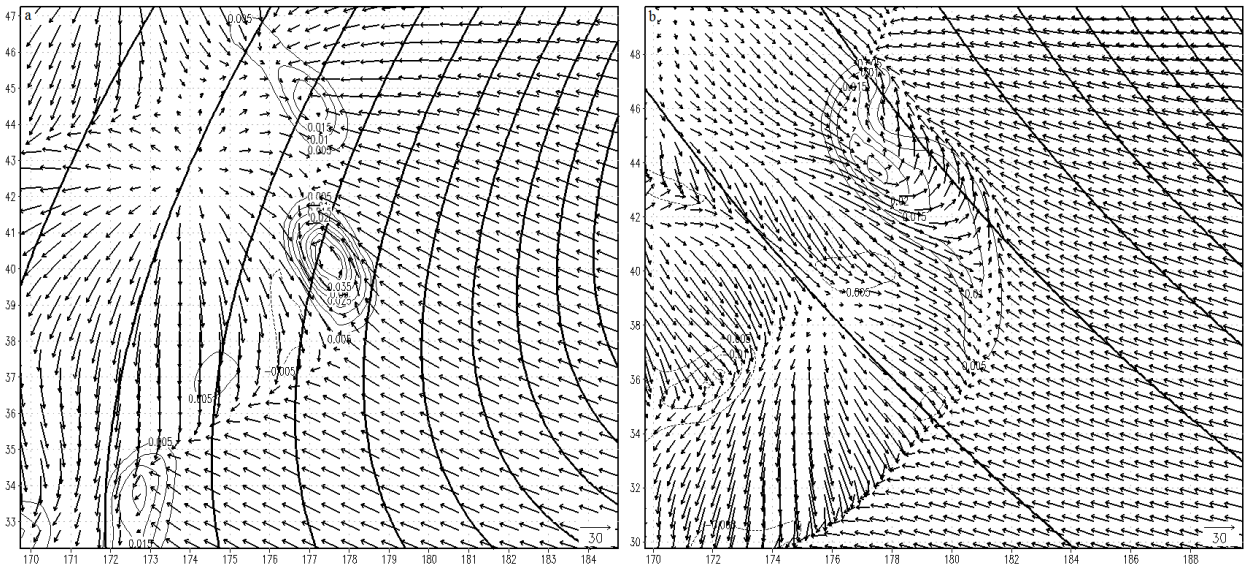

Figure 17. Example of (a) surface closed vortex that meets criteria 1 and (b) cross vortex sheer that does not meet criteria 1.

4.3 Environmental Simulations with Modified Geometry (MTNOMG)

Simulations were performed with mountains of 500, 1000, and 1500 m heights and the mountains were varied through four basic positions such that the semi-major axis is nearly perpendicular to the layer averaged winds (RM45), then nearly parallel (RP45), then two configurations that are roughly 45 deg toward and away (cases 2A, 2B). Rotating the terrain allowed the blocking effect of the terrain to be varied, from strongest (case RM45) to weakest (case RP45). The effective F_w are given in (Table 3), which is determined as follows:

$$F_{we} = F_w \left[\frac{I - Abs(Max(\boldsymbol{U} \cdot \boldsymbol{T}_n, \boldsymbol{C}_s \cdot \boldsymbol{T}_n))}{I} \right]$$

where F_{we} is the effective F_w, I is the interval size defined as: $I \equiv \sum Abs[Max(\boldsymbol{U} \cdot \boldsymbol{T}_n, \boldsymbol{C}_s \cdot \boldsymbol{T}_n)]]$, $\boldsymbol{U}$ is the layer averaged basic wind, $\boldsymbol{C}_s$ is the storm motion vector, $\boldsymbol{T}_n$ is the terrain unit vector normal to the semi-minor axis.

Table 3

Basic Unsaturated Moist Froude numbers, (second row) and Effective for indicated terrain configuration (remaining rows below second).

	500 m	1000 m	1500 m
F_w	1.78	0.89	0.59
RM45	1.91	0.95	0.63
2A	1.93	0.96	0.64
2B	2.76	1.38	0.91
RP45	3.58	1.79	1.19

The environmental modifications induced by the terrain were, as expected, similar to that of the idealized bell shaped mountains in Smith et. al., 2014, denoted as SLR14 hereafter. There was a general region over the terrain where MLCIN (MLCAPE) was reduced (increased) because of a reduction in the distance from the ground to the Lifting Condensation Level (LCL,

Figure 18). These simulations showed alternating increases and decreases in MLCAPE and MLCIN, associated with gravity waves, are seen clearly by the end of the first hour. Vertical vorticity (not shown) indicates the existence of convective rolls over the peak in the simulations with the strongest blocking (i, j, k, l in Figure 18). Closed wake vortices are only seen in the two simulations with the strongest blocking (i, k in Figure 18).

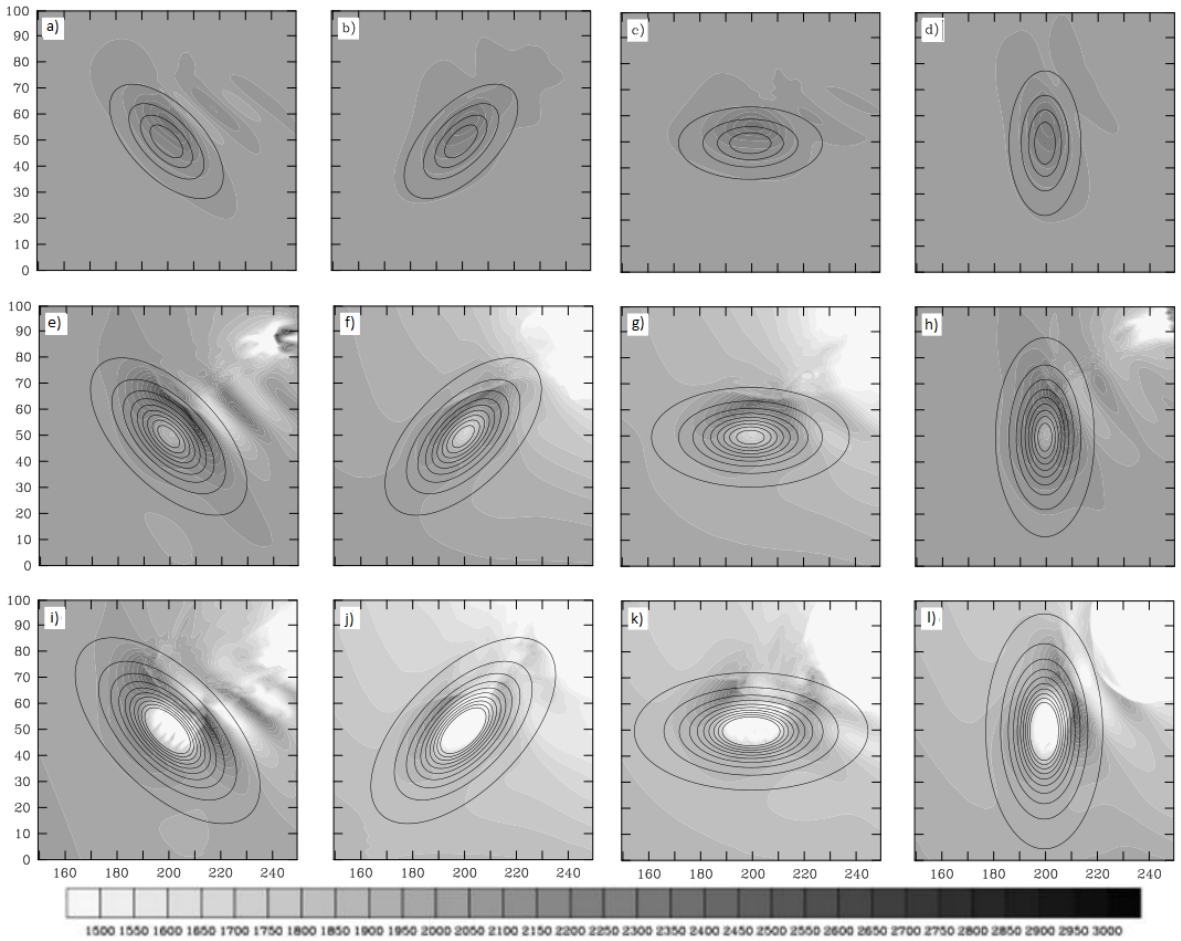

Figure 18. MLCAPE at the simulations third hour for the three varied heights (rows) 500, 1000, and 1500 m from top to bottom and the four different geometries (columns) RM45, RP45, 2A, and 2B from left to right.

As with the BSM of SLR14, supercellular convection was triggered downwind of the mountain in all simulations with mountain heights of 1000 and 1500 m. Interestingly the terrain configuration that produced the strongest blocking, RM45, initiated the convection later that of the other terrain configurations. This lead to a general region of reduced CAPE and increased CIN associated with the cold pool outflow from these storms. The cold pools generated in these simulations do not affect our analysis as our focus is on the windward side of the mountains.

4.4 Effects of Terrain Geometry on Supercell Thunderstorms

4.4.1 Orographic Effects on Supercell Structure and Development. The structure and development of these storms is quite similar, the storms exhibit nearly identical maturing processes and exhibit the structure of the classical High Precipitation Supercell conceptual model (Lemon and Doswell, 1979) by the 105 min. The storms in each of the simulations remain structurally similar until interacting with the terrain directly. Our analysis is started at the 165th and is stopped at the 180th min. This is the last point at which 1000 and 1500 m terrain cases do not interact with the cold pool on the lee side of the mountain. For the most meaningful interpretation comparisons will be grouped by height 500, 1000, and 1500 m terrain heights; M500, M1000, and M1500 respectively. After discussion with the grouped heights some comments will be made about the overall comparisons between the simulations as a whole.

Starting with M500 an immediately noticeable difference between these simulations is that the cloud updraft area in the M500-2A simulation is nearly half the size of the other terrain orientations (Figure 19). In addition to the M500-2A simulation having the narrowest updraft region it also has the strongest gust front (Figure 19). Incidentally this is also the point with the highest precipitation rate (nearly 14 cm hr^{-1}) in M500 (Figure 25c). As the gust front of the M500-2A simulation starts to weaken the cloud updraft area begins to widen (compare Figure

19c and Figure 20c), partially indicative of the cyclic nature of supercell thunderstorms (Burgess et al. 1982; Beck et al. 2006, Klemp and Rotunno 1983; Wicker and Wilhelmson 1995). As the rainfall strengthens in M500-RM45 a stronger gust front is seen developing below the leading edge of the updraft region. The cloud base is the lowest in M500-RP45 and 2A (Figure 19). Additionally as these storms propagate towards the terrain a downdraft is present that advects reflective hydrometeors towards the ground that produces strong reflectivity near the ground (Figure 20).

The 1000 m terrain simulations (M1000) RP45, 2A, and 2B simulations at the 165th min are close to each other in the supercell cycle despite looking quite different which can be seen by comparing the difference in appearance between Figure 21 and Figure 22, especially Figure 21b and Figure 22d). Although close in the supercells cycle there are differences, such as, the general orientation of the updrafts in these simulations is fairly vertical at the 165th min (Figure 21). The M1000-RM45 and 2A storms generate a noticeable eastward tilt this leads to a smaller upwind outflow cloud (Figure 22). The RP45, 2A, and 2B simulations updraft broadens considerably at the mid and upper levels (Figure 22). We also see that the low-level updraft of M1000-2B narrows considerably (Figure 22d) as the storm goes through a period of very strong rain (Figure 25). As the M1000 storms propagate towards the terrain a downdraft advects reflective hydrometeors towards the ground that produces strong reflectivity near the surface (Figure 22).

The 1500 m simulations (M1500) by far had the strongest cold pools which are associated with very high precipitation (Figure 25); moreover these strong cold pools were able to initiate convection. This is immediately noticeable by the area of updraft several kilometers to the west of the main updraft of the supercell thunderstorm (Figure 23a and Figure 23d). This initiated convection may also be a factor of blocking increasing the cold pool depth by stronger

down slope winds, as there is less indication of convective initiation when there is less blocking (Figure 23b and Figure 24b). Although this increases the total amount of precipitation it also weakens the storm considerably (Figure 24d). As the storms propagate over the terrain, the cold pool is blocked by the terrain and the storms are deprived of the additional air lifted by the cold pool and there is a general reduction of the storms updraft as less air is ingested by the storm.

Overall comparison shows, as expected, that M1500 induced more rain both in areal extent and rain rate. Furthermore there is the least variability from storm to storm in M500 even when propagating over the mountain. Higher terrain height generally, but not always, produced more rain (Figure 25), as shown in the comparison of M500 and M1000. The higher rain rates also deepened cold pools that in M1500 initiated additional convection and producing more rain.

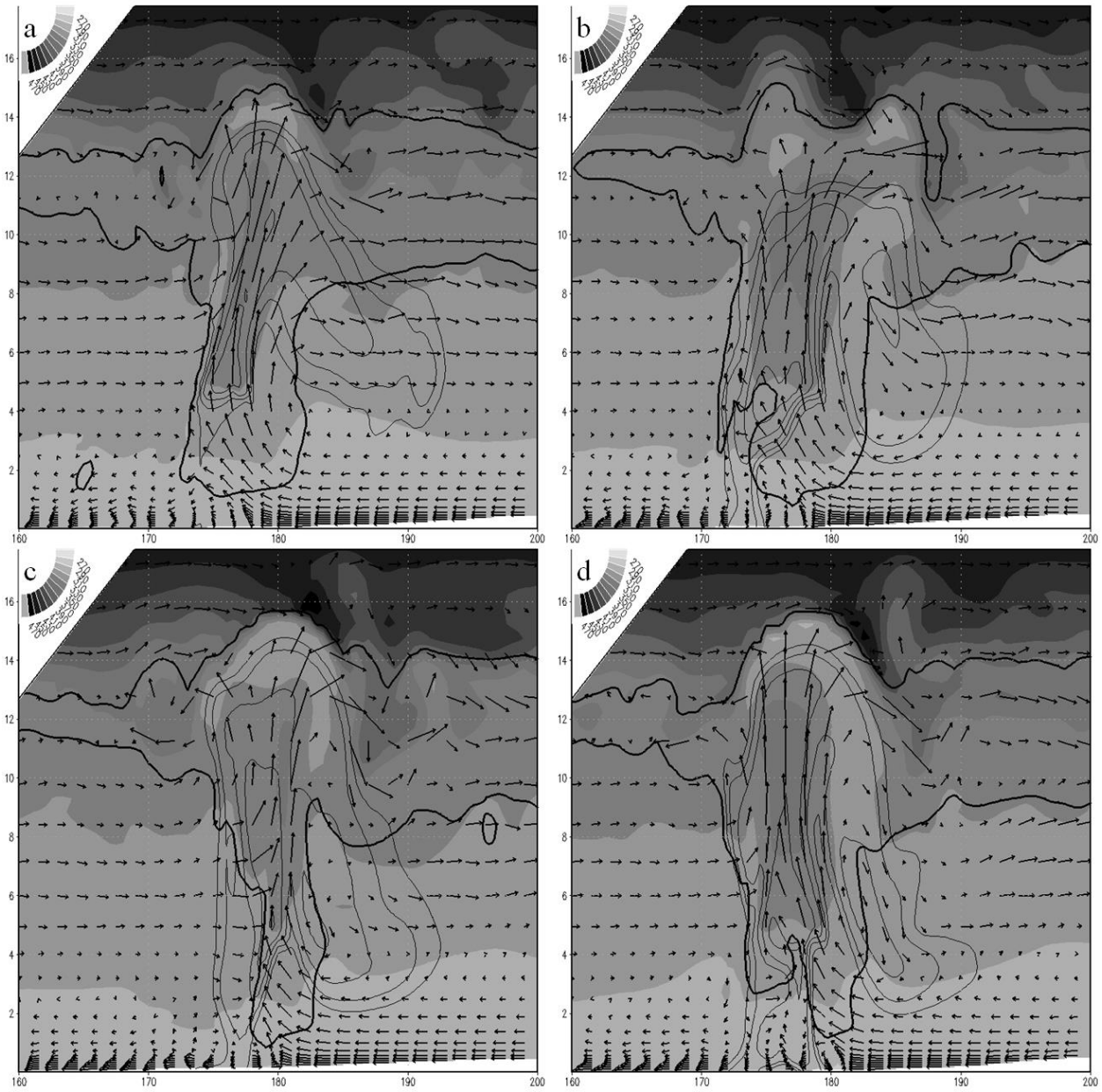

Figure 19. Zonal cross section of theta (shadeing), reflectivity (thin contour), cloud outline (thick contour), and wind vectors, at the 165 min for 500 m mountains and are a) RM45, b) RP45, c) 2A, d) 2B. Reflectivity values start at 50 dBZ and are contoured every 5 dBZ. The Cloud outline is the 0.5 g kg^{-1} cloud and ice mixing ratios. The reference vector is in d and is the same for all panels. Cross section is along the direction of propagation (east-west) and is at the point of maximum UHW.

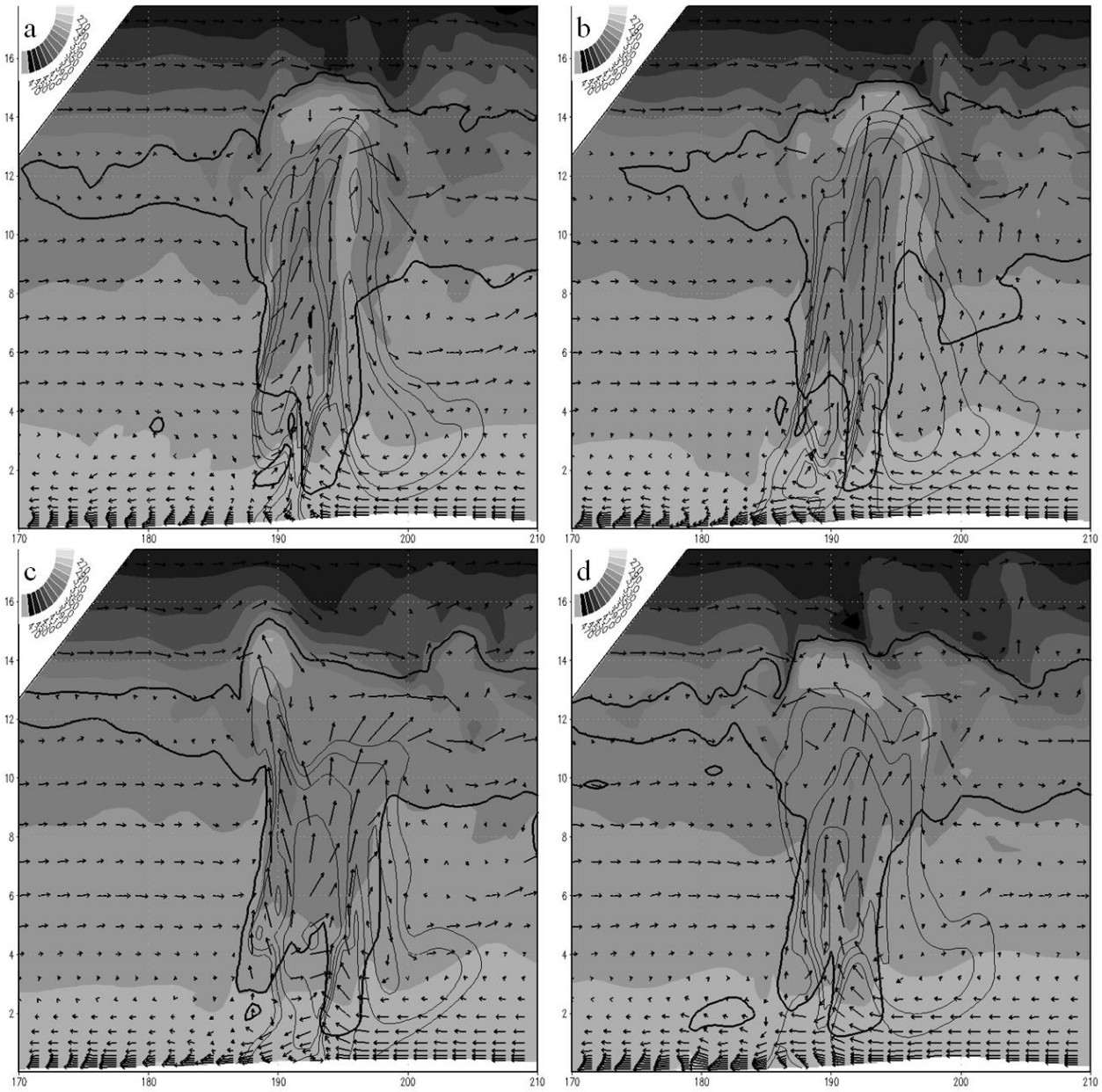

Figure 20. As in Figure 19, but at the 180 min.

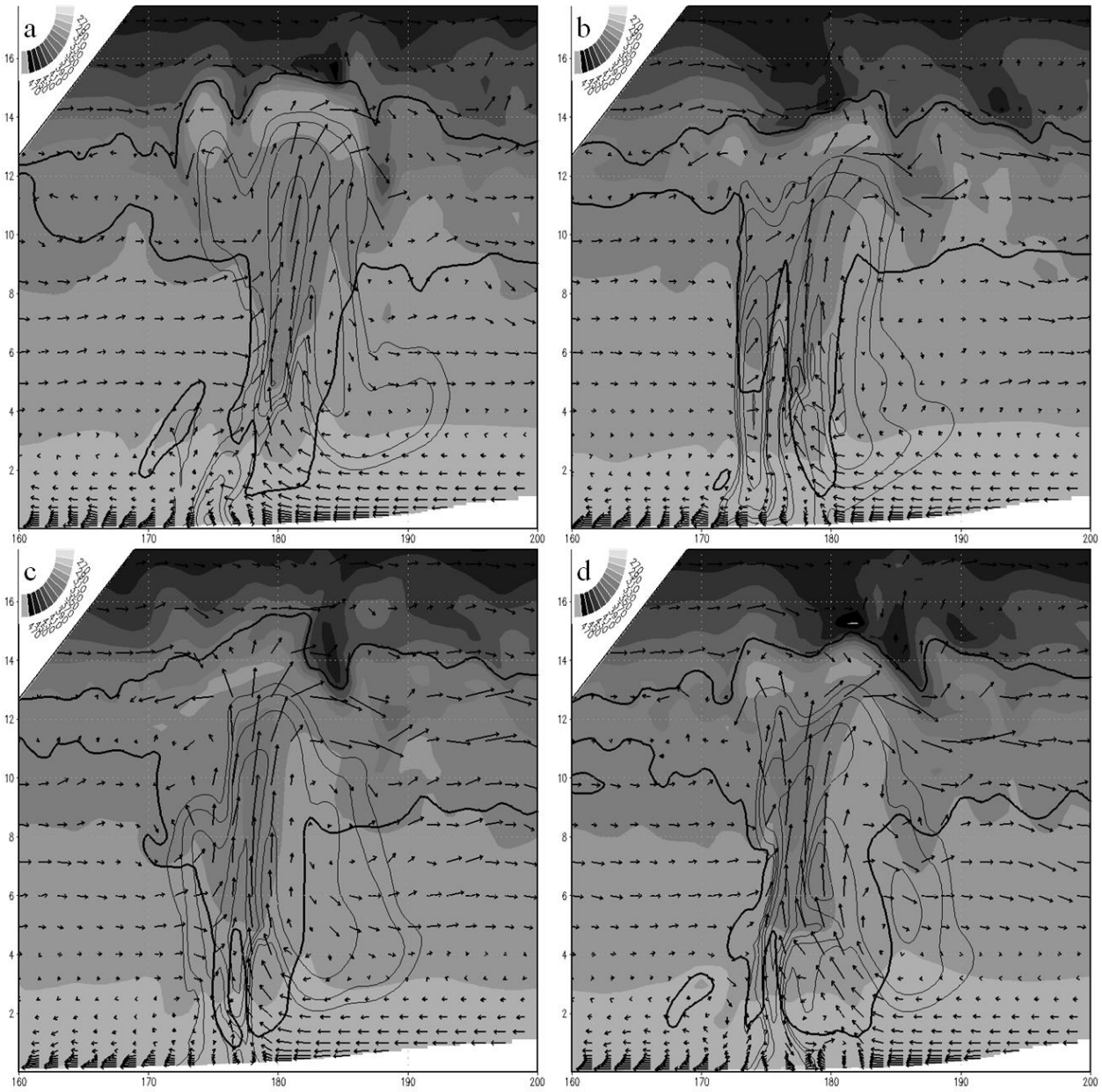

Figure 21. As in Figure 19, but for the 1000 m mountains.

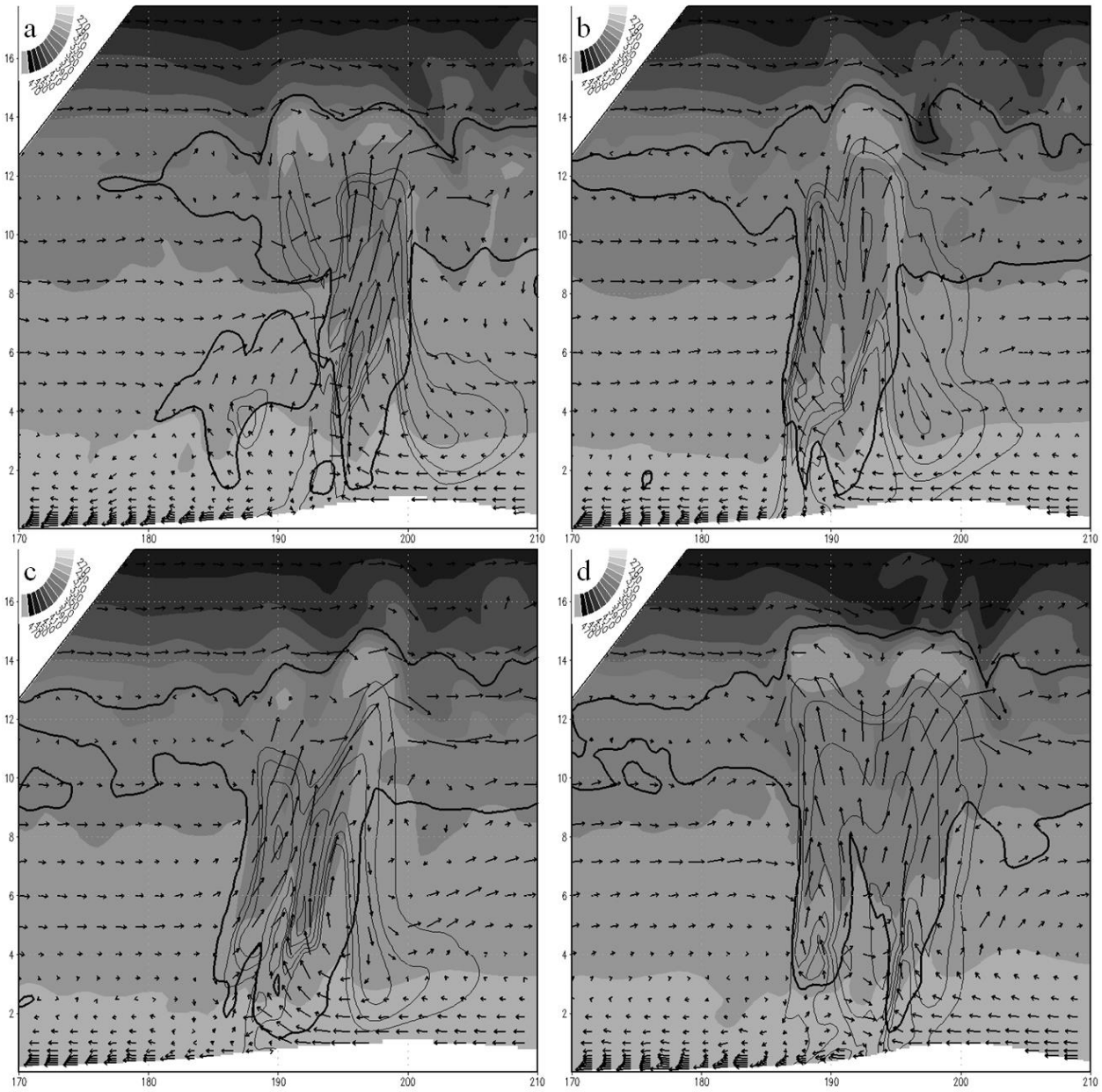

Figure 22. As in Figure 20, but for the 1000 m mountains.

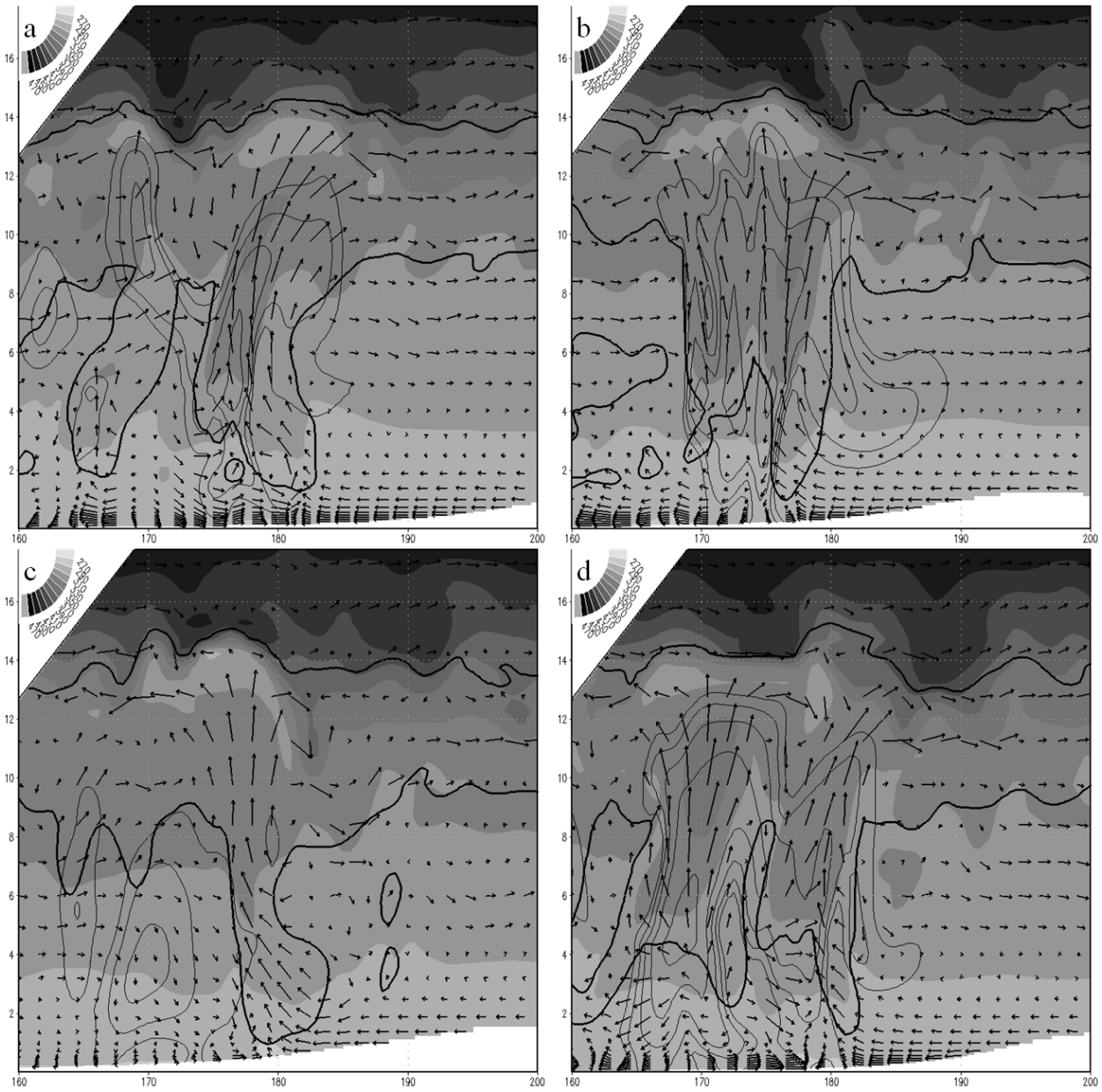

Figure 23. As in Figure 19, but for the 1500 m mountains.

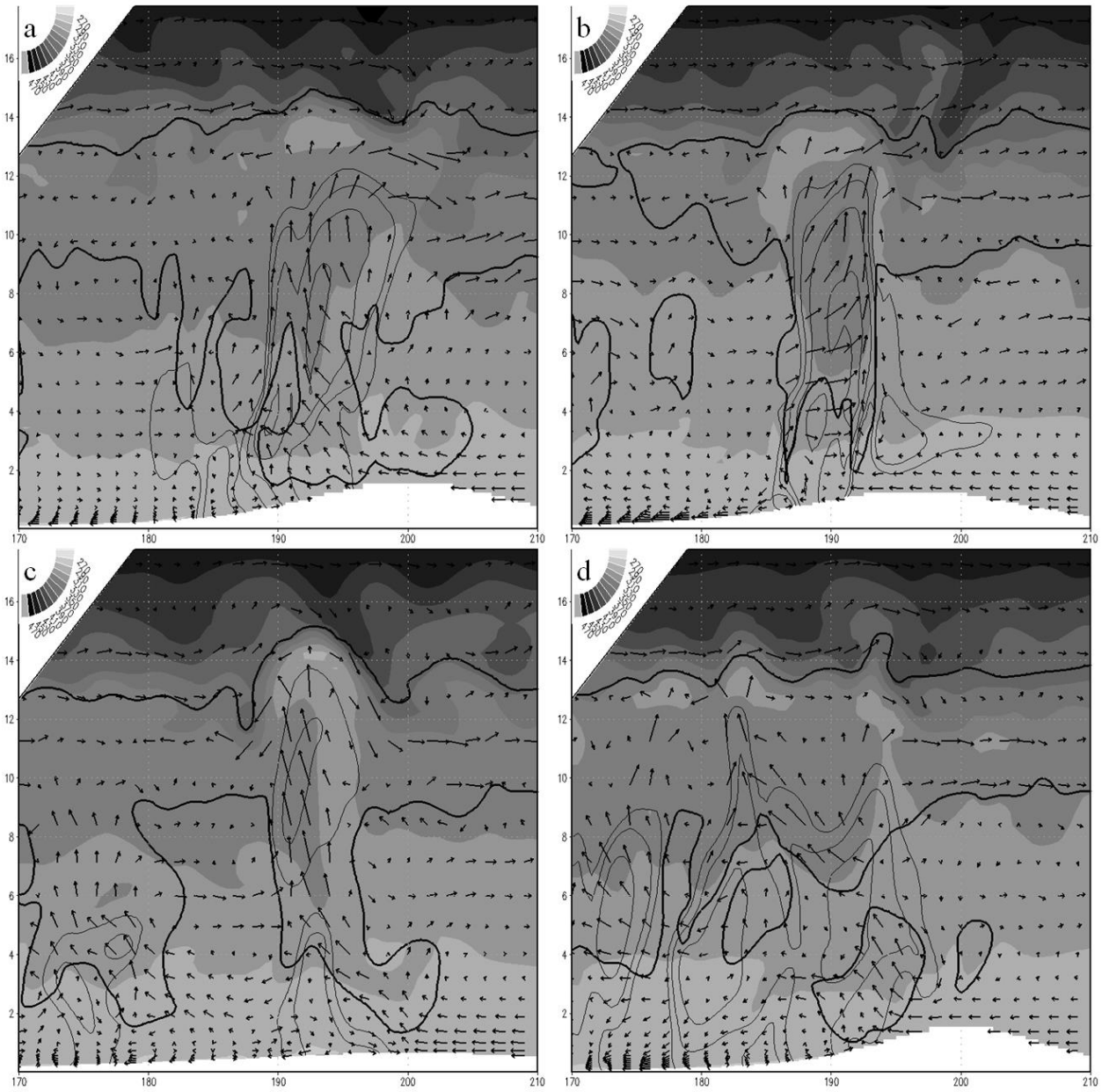

Figure 24. As in Figure 20, but for the 1500 m mountains.

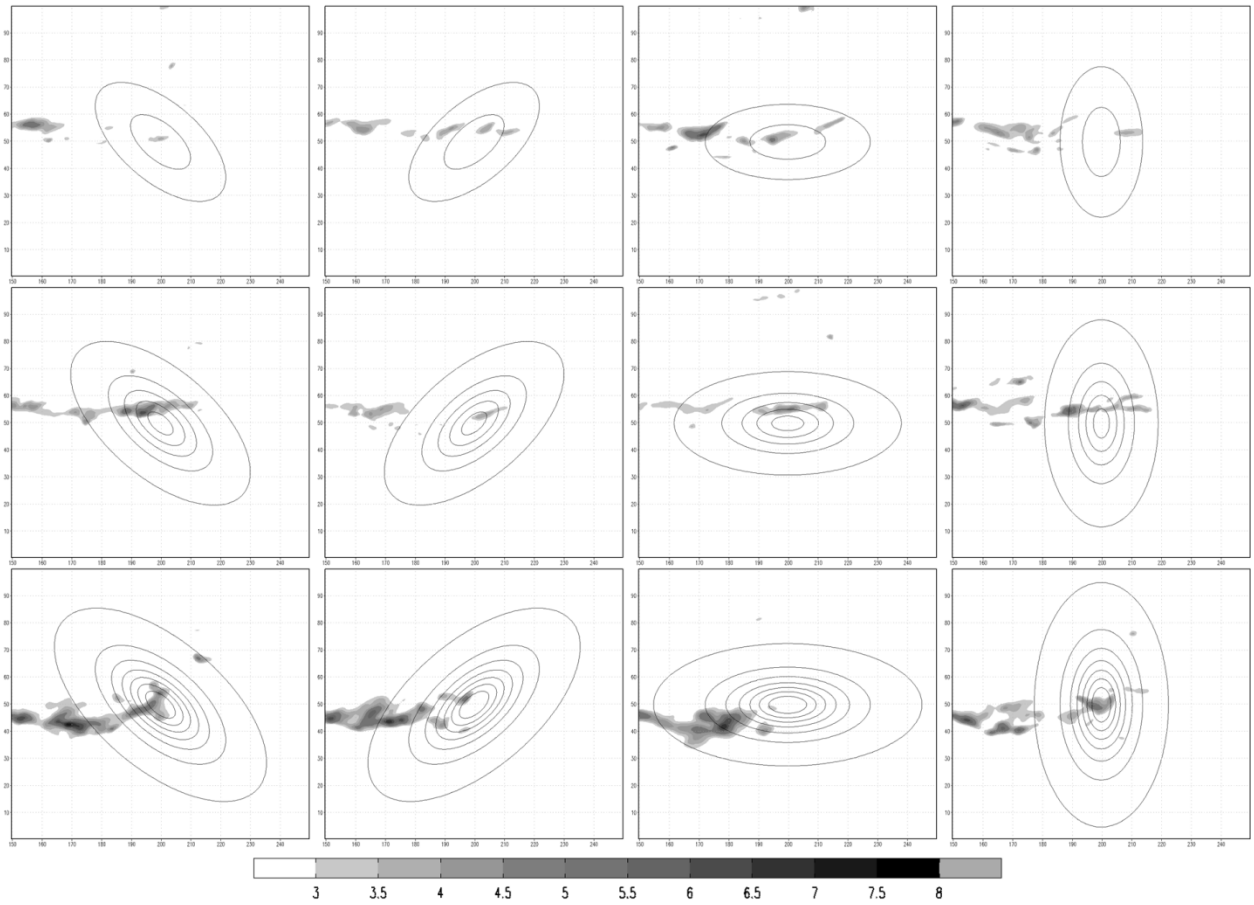

Figure 25. Total accumulated rain out to 210 min. Rows from top to bottom 500, 1000, 1500 m terrain heights. Columns from left to right RM45, RP45, 2A, 2B terrain orientations. Shading starts at 3 cm. Terrain contours start at 100 m and are every 200 m.

4.4.2 Orographic Effects on Supercell Intensity and Tornadogenesis. The intensity of the storms is investigated by looking at the 1 and 5 km updraft strength and the near surface vorticity. Furthermore as discussed in the methodology section we will determine if a storm is tornadic to determine which terrain configuration is most favorable for tornadogenesis. Our analysis will focus on the period from the 165 to 210 min.

The storms in all simulations behaved nearly identical throughout the first two hours with minor variations to the storm location and exhibited cyclic intensification and decay, consistent with observations (Burgess et al. 1982; Beck et al. 2006) and previous numerical simulations

(Klemp and Rotunno 1983; Wicker and Wilhelmson 1995). Terrain also induced slight changes to the period of the storms cycle with intensity peaks nearly the same as a control simulation without terrain (~75 min) for cases with weak blocking and intensity peaks being closer together for cases with strong blocking. The reduction of the cycle appears to be related to additional air directed into the storm by the terrain. The additional air leads to increased rain and a stronger cold pool that helps to reduce the distance between the rear flank down draft and the storms main updraft weakening the storm until it propagates away allowing the storm re-intensify.

At the 165th min the 1 km AGL updraft of M500-2A, 2B, RP45, and RM45 was 15, 14, 12 and 12 m s^{-1}, respectively (Table 4). The downdrafts at this level were 16, 14, 12 and 15 m s^{-1}. The updrafts of M500-2A and 2B weaken slightly by the 180 min most likely due to precipitation loading effects, whereas M500-RP45 and RM45 remain about the same magnitude. The updrafts of M500-2A, 2B, and RP45 continue to weaken as the storm propagates over to the lee side of the mountain. The 5 km AGL updrafts and downdrafts are much less affected by the terrain the 2A, 2B, and RP45 cases intensify slightly giving rise to a slight midlevel stretching. The RM45 simulation updraft weakened considerably with its initial interaction with the terrain then the storm nearly recovered to its pre-interaction strength. Terrain blocking effects actually serve to lower the low-level vorticity in the M500-2B and RP45 simulations (Table 4). Although surface vorticity is increased greatly in the M500-RM45 simulation a vortex never formed and did not meet either of our criteria for being declared tornadic. Even though weakening from the 165th to 180th min the M500-2A and RP45 simulations met both criteria to be deemed a tornadic supercell at the 180th min (*Table 5*).

Table 4

Selected intensity parameters for the four terrain orientations and 3 height levels.

	Time	165 Min			180 min			195 min		
	Case	w 1km	w 5km	Surface Vorticity	w 1km	w 5km	Surface Vorticity	w 1km	w 5km	Surface Vorticity
500 m	2A	14.56	32.95	0.04	12.22	34.83	0.046	10.25	34.3	0.031
	2B	14.01	35.83	0.037	12.35	36.89	0.03	8.44	32.94	0.016
	RP45	12.44	35.48	0.037	12.23	36.71	0.031	9.34	36.29	0.023
	RM45	11.73	39.49	0.019	10.84	35.28	0.058	11.65	36.08	0.052
1000 m	2A	12.77	39.79	0.039	15.09	38.29	0.041	13.45	40.83	0.032
	2B	11.74	32.35	0.049	14.16	35.15	0.035	9.26	37.37	0.037
	RP45	12.18	34.33	0.02	11.99	33.28	0.023	10.56	36.43	0.018
	RM45	12.25	38.08	0.025	14.27	36.22	0.061	12.25	28.64	0.034
1500 m	2A	20.28	30.86	0.038	14.28	27.07	0.037	13.3	32.46	0.036
	2B	18.27	32.91	0.037	11.64	29.61	0.033	11.91	31.24	0.028
	RP45	12.89	31.77	0.045	16.91	34.92	0.048	10.04	29.18	0.026
	RM45	14.48	33.38	0.026	14.51	32.82	0.02	14.5	35.15	0.025

At the 165th min the 1 km AGL updraft of M1000-2A, 2B, RP45, and RM45 was 13, 12, 12 and 12 m s^{-1}, respectively (Table 4). The downdrafts at this level were 16, 15, 14 and 11 m s^{-1}. There is a general strengthening of the low-level updraft as the M1000-2A, 2B, and RM45 approach the terrain and couple with upslope winds. The midlevel 5 km AGL updrafts weaken slightly leading to a slight broadening of the wind field as a light dynamic high forms. The low-level updraft weakens as the storm propagates over to the lee side of the mountain as the midlevel updrafts gradually strengthen. As M1000-2A and RP45 approach the terrain the surface vorticity increases slightly and as was with M500-RM45 the M1000-RM45 increased considerably (Table 4). M1000-2B vorticity weakened. M1000-2B, RP45, and RM45 had

enough vorticity to cross our minimum vorticity threshold of 0.0225 s^{-1}, the vortex was not formed at the LML. M1000-2A simulation met both criteria and is declared tornadic (*Table 5*).

Table 5

Indicates if the supercell thunderstorm met the criteria of the modified tornado detection algorithm to be declared tornadic. (For reference the BSM storms from SLR14 are included).

	BSM	2A	2B	RM45	RP45
M500	Y 180	Y 180	N	N	Y 180
M1000	N	Y 180	N	N	N
M1500	Y 165	Y 165	Y 180	N	Y 165

At the 165th min the 1 km AGL updraft of M1500-2A, 2B, RP45, and RM45 was 13, 12, 12 and 12 m s^{-1}, respectively (Table 4). The downdrafts at this level were 16, 15, 14 and 11 m s^{-1}. M1500-2A and 2B low-level updrafts weaken considerably as they propagate towards the terrain. M1500-RP45 simulation updraft strengthens while the M1500-RM45 stays nearly the same (rounding). The midlevel updraft weakens in M1500-2A and 2B, intensifies in M1500-RP45 case, and remains about the same in M1500-RM45. The vorticity varies quite differently in these simulations as M1500-RM45 weakened as it approached the terrain then intensified slightly. M1500-2A and 2B weakened slightly as it propagated over the terrain. M1500-RP45 simulation intensified slightly as it approached the terrain then weakened significantly as it continued its track over the terrain.

In general, the terrain configuration of case 2A induced tornadogenesis in each of the three terrain heights indicating that this terrain geometry is the most likely to enhance vorticity along the gust front; Followed by the RP45, and the BSM of SLR14, which induced tornadogenesis in the cases with 500 and 1500 m terrain heights. Furthermore, the earlier tornadogenesis with higher terrain us to believe that there is no need to have a steep slope to

enhance vorticity along the gust front, instead the approaching angle toward a terrain may allow the terrain blocking to change the direction of the inflow to enhance vorticity under the main updraft. This is also consistent with our finding that the cyclic nature is shortened in the simulations with increased terrain.

4.4.3 Orographic Effects on Supercell Track. Using the method of SLR14 in which the storm location is identified using the updraft (at 1 km AGL) multiplied by the updraft helicity (1 – 6 km AGL) (UHW). They found that the track is shifted towards the north in their simulations with terrain to the left of the storm's motion; particularly for their 1500 m simulation.

Our investigation using modified terrain geometries has shown that M500 tracks are nearly identical to that of a simulation without terrain, although there are some timing differences but the track is basically the same. Each of the M1500 simulated storms is shifted to the south of the storm's motion and displaced the farthest in M1500-RM45 simulation, and that there is a generally rightward shift with respect to the storm's motion in the tracks as they propagate over the mountains (Figure 26). The general effect of elongating the terrain is to shift the track to left of storm motion early in M1000 and M1500 and toward the right when propagating up to and around the terrain. Although, these simulations were shifted southward this may be a result of a somewhat dissipative/weakening stage as convection is initiated near many of these storms. This may also indicate that approaching the peak slightly to the south will produce a southward shift while the obverse would be true approaching slightly to the north.

Another interpretation using the findings of Lin et. al. (2005) is that our Vortex Froude number in several simulations is greater than 1.5, in their study V_{fr} = 1.5 was a transition point for continuous and discontinuous tracks of cyclones. In addition to our simulated storms having a large V_{fr}, the slope, h/L_x, of our terrain is generally greater than that in Lin et. al. (2005) in some

cases an order of magnitude larger. The steep terrain and the large V_{fr} in combination with the fast interaction time (~10 min to cross the entire mountain) and the terrain induced vorticity being 2-3 orders in magnitude smaller than the storms vorticity show that there is a negligible contribution to track deflection from terrain induced vorticity. This last interpretation is another area that needs further investigation as the time and length scales and maintenance mechanisms are very different between tropical cyclones, and supercells and tornadoes.

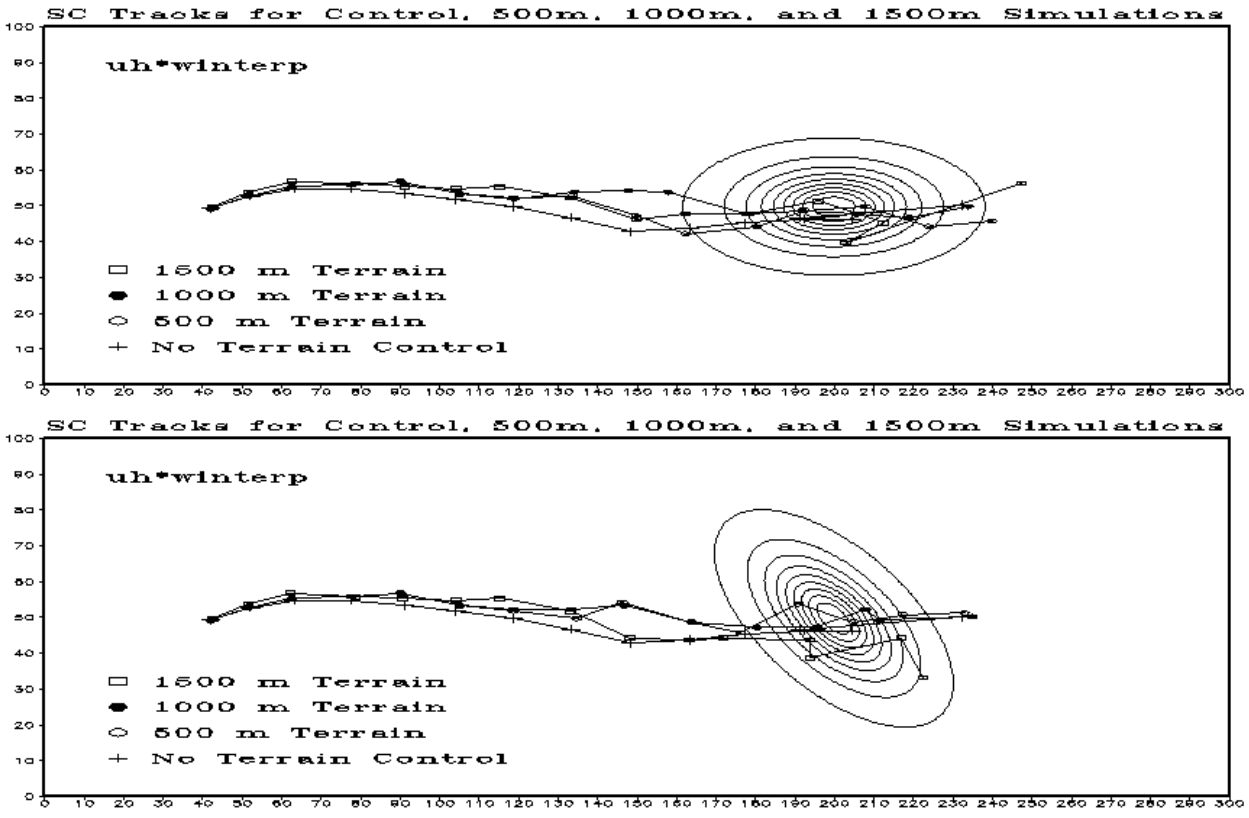

Figure 26. Tracks for a) the 1500 m 2A simulation and b) the 1500 m RM45 simulation.

4.5 Concluding Remarks

The effects of elongated bell-shaped mountains, with different orientations and heights, on supercell thunderstorms were investigated in this study. The terrain produced gravity waves that modified the lee side of the terrain by generating alternating reductions and increases in the

amounts of moisture, MLCAPE, and MLCIN. These gravity waves were strong enough to initiate convection in all of the 1000 m and 1500 m simulations. It is interesting to note that despite the RM45 orientation having the strongest blocking (in relation to the mean wind) it initiated convection later than M1000 and m1500-2A, 2B, and RP45. Convection associated with these storms was initiated from about the 90 – 180 min with the earliest initiated in the 2A followed by RP45, 2B, RM45 sequentially. The effects of reduced CAPE and increased CIN eventually would reduce the amount of energy available to the storm and was unable to sustain the storm, although our analysis was concluded before this happened and these storms did not reach this point).

The structure and development is nearly identical in all simulations out to the 75th min slight variations become insipient near the 90 min (about half way between the location of the initial warm bubble and the terrain peak). When comparing the M500 group there is the least variability between RM45, RP45, 2A, and 2B configurations (although there are differences between the simulations) this is understandable as the M500 simulations all had F_w >1.5. The largest difference is between the 2A and other simulations where the updraft is considerably smaller and weaker at the 165 min, just after a period of very high rain fall. The 1000 m simulations exhibited variations in their intensity cycle that produced storms with similar structure at different times. Similar to the significate narrowing of the updraft in the 500 m 2A case there is a significant narrowing of updraft cores in the 1000 m RM45 and 2B cases after they undergo a similar period of very high rain fall. The 1500 m simulations behaved quite differently from the 500 and 1000 m cases experiencing extremely high rain fall rates and areal coverage, that in turn generated cold pools deep enough to initiate convection over the cold pool. The net effect of the additional convection was that the two storms started to “compete” with

each other to ingest air and had a general weakening effect overall but help to produce more rain. Nearly all of the 1500 m simulations had a period where the rain rate approached 16 cm h^{-1}.

Our intensity investigation focused on the 1 and 5 km updrafts and the surface vorticity. The intensity of supercells was cyclic in all simulations; however the period between intensity peaks were reduced in cases were more air was directed into the storm's inflow as compared to the no mountain (NMTN) control case. The increased (decreased) air flow created differences in the distributions of hydrometeors and increased (decreased) the rainfall rate and areal extent. This allowed the cold pool to be stronger in the simulations with more rain, most notably when the cold pools of the 1500 m storms became deep enough to initiate convection.

In addition, looking at these indicators of storm intensity we used a slightly stricter form of the National Weather Service's tornado detection algorithm to decide which terrain configuration would be most favorable for tornadogenesis. We found that despite being able to produce stronger blocking effects, the 1000 m mountains were generally the least favorable to tornadogenesis, with a tornado declared in only the M1000-2A case. The 1500 m mountains were most favorable for tornadogenesis, with a tornado declared in all cases except M1500-RM45. Surprisingly the RM45 configuration, the case with the strongest blocking in relation to the layer averaged mean wind, did not produce any tornadoes; this showed that it took more than blocking alone to generate a closed vortex throughout a depth of 1.5 km with sufficient winds to meet our criteria.

Looking at the effective Froude number we have seen that the basic effect of modifying the terrain geometry is to increase the basic Froude number, significantly in the RP45 configuration. The effective Froude number does give rise to a correct ordering of the geometries according to how much blocking is expected from the given configurations. However, even

using the effective Froude number we still do not get a clear picture of how to effectively use it to determine which cases are more likely to enhance tornadogenesis in supercell thunderstorms, as we have seen that although the 2A geometry enhances tornadogenesis potential it has nearly an identical effective Froude number.

We have shown that additional air could modify supercellular convective life cycle through the redirection of additional air into the storms inflow. This additional air also increases the amount of rain in simulations with higher terrain deepening the cold pool (to the point that it may initiate convection in the 1000 m and 1500 m cases). This is of interest to now/forecasters as the increased rain can produce severe local flooding. Also of interest to now/forecasters is that terrain blocking effects alone are not sufficient enough to enhance tornadogenesis, but there has to be an increased likelihood of the terrain blocking effects to enhance the vorticity along the gust front and enhance the formation of a closed vortex beneath the main updraft. Furthermore as high terrain produced a dramatic increase in vorticity this may lead to faulty attribution of damage to a tornado.

We investigated the proposed tracking method of SLR14 and found that with respect to modifying the orientation of elongated bell-shaped mountains using their UHW parameter for tracking a supercell thunderstorm was not robust. It was noted that this may be due to the impinging location slightly north or south could produce a northward or southward tendency for propagation. An alternate explanation offered that the Vortex Froude number was close to a transition region.

Areas where this study could be extended are incorporation of real terrain in these idealized simulations, such as configuring a domain that utilizes the terrain areas identified by Broyles and Crosbie (2004). Further, the flow regimes for these terrains using the WK82

sounding could be investigated; especially since some unexpected environmental evolutions formed (e.g. convection was initiated sooner in RP45 than RM45). This area still has much to be researched and additional attention is needed.

CHAPTER 5

Discussion and Future Research

This research focused on the effect of initially round idealized bell-shaped mountains that were varied with height. Following elongated bell-shaped mountains of varying heights and orientations were investigated. It is found that the MNT simulations (both round and elongated) produced strong environmental modifications on the Lee side of the mountain. In each of the M1000 and M1500 simulations supercelluar convection was initiated by mountain waves. The initiated storm produced a cold pool that arrived at the mountain and started to become a significant (greater than 10% reduction in CAPE) influence ~225 min into the simulation.

Supercelluar development and structure are altered when simulations include terrain through terrain blocking effects increasing the amount of available air for the storm to ingest. The additional air modifies hydrometeor distributions favoring ice species and producing higher rainfall amounts. Further the increased rain shortens the cyclic nature of the storm by causing the storms cold pool to push the storms down draft into closer proximity to the main updraft.

It was found that supercelluar storms approaching terrain could have a greater tornadogenesis potential when the storm motion vector was approximately parallel to the semi-major axis of elongated terrain. Overall the approach angle is more important for elongated terrain than the mountain height. After the approach angel terrain height becomes an increasingly important factor in supercullular tornadogenesis. Interestingly, the M500 simulations (both round and elongated) were more likely to produce a tornadic phase than the M1000 simulations.

The effects of idealized bell-shaped mountains of various heights on supercell thunderstorms are first studied. The mountains produced gravity waves that modified the

downwind environment by producing alternating reductions and increases in the amounts of moisture, MLCAPE, and MLCIN. The simulations with higher mountains produced gravity waves that had enough vertical motion to initiate convection. Cold outflow from these storms reached the lee side at approximately the 225 and 180 min for the M1000 and M1500 simulations, respectively. Although these storms produced large environmental modifications our analysis was focused before these effects could influence the investigated supercells.

Several combinations of variables were used to create parameters for the identification of a supercell's location. Although the updraft helicity (UH) indicated the general vicinity of the supercell the identified track that was rather erratic. Other parameters that were used based on the characteristics of supercells yielded smoother tracks; however the maximum UHW (UH multiplied by the updraft velocity) produced the smoothest tracks and tracks that were the most similar far from the mountain where the terrain effects are minimal. Using the maximum UHW we identified that increasing the mountain height shifted the tracks of supercells towards the north. Looking at the vorticity budget it is found that terrain generated vorticity has a negligible effect on modifying the track of the storm as it is 2-3 orders of magnitude smaller than that of the supercell thunderstorm itself.

The intensity of supercells was cyclic in all simulations; however the period between intensity peaks were reduced in MTN as compared to NMTN. The intensity, structure and development of the storms were mainly a result of the mountain directing an increased amount of environmental air into the storms inflow. This created differences in the distributions of hydrometeors and increased the rainfall areal extent. This allowed the cold pool to be stronger in the MTN simulations, most notably when the cold pool undercut the M1500 storm.

Airflow was also modified such that vorticity was generated and/or intensified when approaching the mountain peak. The near surface rotation of the M500 (F_w=1.78) storm intensified as it approached the mountain peak. The M1000 (F_w=0.89) storms propagation speed was reduced as it crossed the terrain, which allowed the storm's rear flank downdraft to run into the storms low-level updraft and reduced the near surface vorticity greatly. The M1500 (F_w=0.59) storm experienced a greater reduction storm motion, however, its' rear flank downdraft was farther away from its updraft and its intensity was not affected in the same manner as M1000. The M1500 storm propagated around to the north of the mountain peak and its cold pool worked in conjunction with the terrain to block the storm's inflow and causing the storm to weaken considerably until it propagated into the lee side convergence region.

We have shown that blocking effects may direct additional air into the storms inflow and enhance low-level vorticity along the gust front and that these blocking effects are far more important that the than the environmental modifications, especially since we observed these differences before the storm even interacted with the environmental modifications on the lee side of the mountain. The direction of additional moist air into the storm is particularly of interest to now/forecasting because this increases the precipitation amount and was observed far from the mountain and could increase the likelihood of flash flooding. The M1000 and M1500 simulations initiated supercellular convection that reduced the MLCAPE and increased the MLCIN far more than the gravity waves excited by the mountain and indeed when the simulated storms propagated into this region they quickly dissipated.

Further we studied the effects of elongated bell-shaped mountains, with various orientations and heights, on supercell thunderstorms were discussed. The terrain produced gravity waves that modified the lee side of the terrain by generating alternating reductions and

increases in the amounts of moisture, MLCAPE, and MLCIN. These gravity waves were strong enough to initiate convection in all of the 1000 m and 1500 m simulations. It is interesting to note that despite the RM45 orientation having the strongest blocking (in relation to the mean wind) it initiated convection later than M1000 and m1500-2A, 2B, and RP45. Convection associated with these storms was initiated from about the 90 – 180 min with the earliest initiated in the 2A followed by RP45, 2B, RM45 sequentially. The effects of reduced CAPE and increased CIN eventually would reduce the amount of energy available to the storm and was unable to sustain the storm, although our analysis was concluded before this happened and these storms did not reach this point.

The structure and development is nearly identical in all simulations out to the 75^{th} min slight variations become insipient near the 90 min (about half way between the location of the initial warm bubble and the terrain peak). When comparing the M500 cases there is the least variability between RM45, RP45, 2A, and 2B configurations (although there are differences between the simulations). The largest difference is between the 2A and other simulations where the updraft is considerably smaller and weaker at the 165 min, just after a period of very high rain fall. The M1000 cases exhibited variations in their intensity cycle that produced storms with similar structure at different times. Similar to the significate narrowing of the updraft in the M500-2A case there is a significant narrowing of updraft cores in the M1000- RM45 and M1000-2B cases after they undergo a similar period of very high rain fall. The M1500 cases behaved quite differently from the M500 and M1000 cases experiencing extremely high rain fall rates and areal coverage, that in turn generated cold pools deep enough to initiate convection over the cold pool. The net effect of the additional convection was that the two storms started to "compete" with each other to ingest air and had a general weakening effect overall but help to

produce more rain. Nearly all of the M1500 cases had a period where the rain rate approached 16 cm h^{-1}.

Our intensity investigation focused on the 1 and 5 km updrafts and the surface vorticity. The intensity of supercells was cyclic in all simulations; however the period between intensity peaks were reduced in cases were more air was directed into the storm's inflow as compared to the no mountain (NMTN) control case. The increased (decreased) air flow created differences in the distributions of hydrometeors and increased (decreased) the rainfall rate and areal extent. This allowed the cold pool to be stronger in the simulations with more rain, most notably when the cold pools of the M1500 cases became deep enough to initiate convection.

In addition, looking at these indicators of storm intensity we used a slightly stricter form of the National Weather Service's tornado detection algorithm to decide which terrain configuration would be most favorable for tornadogenesis. We found that despite being able to produce stronger blocking effects, the 1000 m mountains were generally the least favorable to tornadogenesis, with a tornado declared in only the M1000-2A case. The 1500 m mountains were most favorable for tornadogenesis, with a tornado declared in all cases except M1500-RM45. Surprisingly the RM45 configuration, the case with the strongest blocking in relation to the layer averaged mean wind, did not produce any tornadoes; this showed that it took more than blocking alone to generate a closed vortex throughout a depth of 1.5 km with sufficient winds to meet our criteria.

Looking at the effective Froude number we have seen that the basic effect of modifying the terrain geometry is to increase the basic Froude number, significantly in the RP45 configuration. The effective Froude number does give rise to a correct ordering of the geometries according to how much blocking is expected from the given configurations. However, even

using the effective Froude number we still do not get a clear picture of how to effectively use it to determine which cases are more likely to enhance tornadogenesis in supercell thunderstorms, as we have seen that although the 2A geometry enhances tornadogenesis potential it has nearly an identical effective Froude number.

We have shown that additional air could modify supercellular convective life cycle through the redirection of additional air into the storms inflow. This additional air also increases the amount of rain in simulations with higher terrain deepening the cold pool (to the point that it may initiate convection in the M1000 and M1500 cases). This is of interest to now/forecasters as the increased rain can produce severe local flooding. Also of interest to now/forecasters is that terrain blocking effects alone are not sufficient enough to enhance tornadogenesis, but there has to be an increased likelihood of the terrain blocking effects to enhance the vorticity along the gust front and enhance the formation of a closed vortex beneath the main updraft. Furthermore as high terrain produced a dramatic increase in vorticity this may lead to faulty attribution of damage to a tornado.

We investigated the proposed tracking method of SLR14 and found that with respect to modifying the orientation of elongated bell-shaped mountains using their UHW parameter for tracking a supercell thunderstorm was not robust. It was noted that this may be due to the impinging location slightly north or south could produce a northward or southward tendency for propagation. An alternate explanation offered that the Vortex Froude number was close to a transition region.

Areas where this study could be extended in the future are to vary the arrival time of the storm to investigate the terrain effects on developing storms. The storms approaching position could be modified to test the robustness of our conclusion that the terrain blocking effects are

dominative over other factors. Further areas where this study could be extended are incorporation of real terrain in idealized simulations, such as configuring a domain that utilizes the terrain areas identified by Broyles and Crosbie (2004). Further, the flow regimes for these terrains using the WK82 sounding could be investigated; especially since some unexpected environmental evolutions formed (e.g. convection was initiated sooner in RP45 than RM45). Incorporation of soundings from actual tornadic events could also be used to initialize the simulations with idealized bell shaped mountains round or elongated and with modified orientations. This area still has much to be researched and additional attention is needed.

References

Adlerman, E. J., K. K. Droegemeier, and R. P. Davies-Jones, 1999: A numerical simulation of cyclic mesocyclogenesis. *J. Atmos. Sci.*, **56**, 2045–2069.

Adlerman, E. J. and K. K. Droegemeier, 2002: The sensitivity of numerically simulated cyclic mesocyclogenesis to variations in model physical and computational parameters. *Mon. Wea. Rev.*, **130**, 2671–2691.

Adlerman, E. J. and K. K. Droegemeier, 2005: The dependence of numerically simulated cyclic mesocyclogenesis upon environmental wind shear. *Mon. Wea. Rev.*, **133**, 3595–3623.

Beck, J. R., Schroeder, J. L., and Wurman, J. M., 2006: High-resolution, dual-Doppler analyses of the 29 May 2001 Kress, Texas, cyclic supercell. Mon. Wea. Rev., **134**, 3125–3148.

Bluestein, H. B., 2000: A tornadic supercell over elevated, complex terrain: The Divide, Colorado, storm of 12 July 1996. *Mon. Wea. Rev*., **128**, 795-809.

Bosart, L. F., Seimon, A., LaPenta, K. D., and Dickinson, M. J., 2006: Supercelltornadogenesis over complex terrain: The Great Barrington, Massachusetts, tornado on 29 May 1995. *Wea. Forec.*, **21**, 897-922.

Brooks, H. E., C. A. Doswell III, and R. B. Wilhelmson, 1994: The role of midtropospheric winds in the evolution and maintenance of low-level mesocyclones. *Mon. Wea. Rev.*, **122**, 126–136.

Browning, K. A. and F. H. Ludlam, 1962: Airflow in convective storms. *Quart. J. Roy. Meteor. Soc.*, **88**, 117–135.

Broyles, C. and C. Crosbie, 2004: Evidence of smaller tornado alleys across the United States based on a long track F3-F5 tornado climatology study from 1880-2003. 22nd Conf. Severe Local Storms, P5.6.

Bryan G. H., and Fritsch, J. M., 2002: A benchmark simulation for moist nonhydrostatic numerical models. Mon. Wea. Rev., **130**, 2917–2928.

Bunkers, M. J., M. R. Hjelmfelt, and P. L. Smith, 2006: An observational examination of long-lived supercells. Part I: Characteristics, evolution, and demise. *Wea. Forec*., **21**, 673-688.

Bunkers, M. J., J. S. Johnson, L. J. Czepyha, J. M. Grzywacz, B. A. Klimowski, and M. R. Hjelmfelt, 2006: An observational examination of long-lived supercells. Part II: Environmental conditions and forecasting. *Wea. Forec.*, **21**, 689-714.

Byers, H. R. and R. R. Braham, 1949: The Thunderstorm Project. U.S. Weather Bureau, Washington, DC, 287.

Burgess D. W., Wood, V. T., and Brown, R. A., 1982: Mesocyclone evolution statistics. Preprints, 10th Conf. on Severe Local Storms, Omaha, NE, Amer. Meteor. Soc., 422–424.

Chen, S.-H. and Lin, Y.-L., 2005: Effects of the basic wind speed and CAPE on flow regimes associated with a conditionally unstable flow over a mesoscale mountain. J. Atmos. Sci., **62**, 331-350.

Chen, C., Y.-L., Lin, N. Hsu, C. Liu, and C. Chen, 2011: Orographic effects on localized heavy rainfall events over southwestern Taiwan on 27 and 28 June 2008 during the post-Mei-Yu period, *Atmos. Res.*, doi:10.1016/j.atmosres.2011.04.004.

Chiao, S., Lin, Y.-L., and Kaplan, M. L., 2004: Numerical Studey of the Orographic Forcing of Heavy Precipitation during MAP IOP-2B, *Mon. Wea. Rev*., **132**, 2184-2203.

Chu, C.-M., and Lin, Y.-L., 2000: Effects of Orography on the Generation and Propagation of Mesoscale Convective Systems in a Two-Dimensional Conditionally Unstable Flow, *J. Atmos. Sci.*, **57**, 3817-3837.

Ćurić, M., Janc, D., Vučković, V., 2003a. The effects of a river valley on an isolated cumulonimbus cloud development. Atmos. Res., 66: 123–139.

Ćurić, M., Janc, D., Vučković, V., 2007: Numerical simulation of a Cb cloud vorticity. Atmos. Res., **83**, pp. 427–434.

Ćurić, M., Janc, D., Vučković, V., 2008. Precipitation change from a cumulonimbus cloud downwind of a seeded target area. J. Geophys. Res., 113: D11215, DOI: 10.1029/2007JD009483.

Ćurić M., Janc D., 2011: Differential heating influence on hailstorm vortex pair evolution. Q. J. R. Meteorol. Soc., **138**, pp. 72–80. DOI:10.1002/qj.918.

Darkow G. L. and J. C. Roos, 1970: Multiple tornado producing thunderstorms and their apparent cyclic variations in intensity. Preprints, 14th Conf. on Radar Meteorology, Tucson, AZ, *Amer. Meteor. Soc.*, 305–308.

Davies-Jones, R. P. and H. E. Brooks, 1993: Mesocyclogenesis from a theoretical perspective. *The Tornado: Its Structure, Dynamics, Prediction, and Hazards*, Geophys. Monogr., No. 79, Amer. Geophys. Union, 105–114.

Dean, A. R. and D. A. Imy, 2006: A look at the tornado report and watch climatology for the continental United States from 1986-2005, 23rd Conference on Severe Local Storms, Amer. Meteor. Soc., P2.2.

Deardorff, J.W., 1980: Stratocumulus-capped mixed layers derived from a three dimensional model. Bound.-Layer Meteor., **18**, 495–527.

Dowell, D. C. and H. B. Bluestein, 1997: The Arcadia, Oklahoma, storm on 17 May 1981: Analysis of a supercell during tornadogenesis. *Mon. Wea. Rev.*, **125**, 2562–2582.

Dowell, D. C. and H. B. Bluestein, 2002A: The 8 June 1995 McLean, Texas, storm. Part I: Observations of cyclic tornadogenesis. *Mon. Wea. Rev.*, **130**, 2626–2648.

Dowell, D. C. and H. B. Bluestein, 2002B: The 8 June 1995 McLean, Texas, storm. Part II: Cyclic tornado formation, maintenance, and dissipation. *Mon. Wea. Rev.*, **130**, 2649–2670.

Droegemeier, K. K., S. M. Lazarus, and R. P. Davies-Jones, 1993: On the rotation and propagation of simulated supercell thunderstorms. *Mon. Wea. Rev.*, **121**, 2005–2029.

Dudhia, J., 1993: A nonhydrostatic version of the Penn State/NCAR mesoscale model: validation tests and simulation of an Atlantic cyclone and cold front. Mon. Wea. Rev. **121**, 1493 – 1513.

Durran, D.R., Klemp, J.B., 1983: A compressible model for the simulation of moist mountain waves, Mon. Wea. Rev., **111**, pp. 2341–2361.

Epifanio, C.C., D.R. Durran, 2002: Lee-vortex formation in free-slip stratified flow over ridges. Part I: comparison of weakly nonlinear inviscid theory and fully nonlinear viscous simulations. *J. Atmos. Sci.*, **59**, 1153–1165.

Emanuel, K.A., 1994, Atmospheric Convection, Oxford University Press, 580 pp.

Frame, J., and Markowski, P., 2006: The interaction of simulated squall lines with idealized mountain ridges. *Mon. Wea. Rev.*, **134**, 1919-1941.

Fujita, T., 1958: Mesoanalysis of the Illinois tornadoes of 9 April 1953. *J. Meteor.*, **15**, 288–296.

Gaffin, D. M., and S. S. Parker, 2006: A climatology of synoptic conditions associated with significant tornadoes across the southern Appalachian region. *Wea. Forec.*, **21**, 735-751.

Gal-Chen, T., and Somerville, R.C.J., 1975: On the use of a coordinate transformation for the solution of the Navier-Stokes equations. J. Comput. Phys., **17**, 209-228, doi:10.1016/0021-9991(75)90037-6.

Gilmore, M. S. and L. J. Wicker, 1998: The influence of midtropospheric dryness on supercell morphology and evolution. *Mon. Wea. Rev.*, **126**, 943–958.

Grell, G.A., Dudhia, J., Stauffer, D.R., 1995. A description of the fifth-generation Penn State/NCAR mesoscale model (MM5), NCAR Tech. Note NCAR/TN-398 + STR.

Hocker, J. E., and J. B. Basara, 2008a: A 10-year spatial climatology of squall line storms across Oklahoma. *Int'l J. Clim.*, **28**, 765-775.

Hocker, J. E., and J. B. Basara, 2008b: A Geographic Information Systems–Based Analysis of Supercells across Oklahoma from 1994 to 2003. *J. Appl. Meteor. Clim.*, **47**, 1518-1538.

Homar, V., 2003: Tornadoes over complex terrain: an analysis of the 28th August 1999 tornadic event in eastern Spain. *Atmos. Res.*, **67-68**, 301-317.

Kain, J. S., Weiss, S.J., Bright, D.R., Baldwin, M.E., Levit, J.J., Carbin, G.W., Schwartz, C.S., Weisman, M.L., Droegemeier, K.K., Weber, D.B., Thomas, K.W., 2008: Some practical considerations regarding horizontal resolution in the first generation of operational convection-allowing NWP. *Wea. Forec.*, **23**, 931–952.

Kirkpatrick, J. C., E. W. McCaul, Jr., and C. Cohen, 2007: The motion of simulated convective storms as a function of basic environmental parameters. *Mon. Wea. Rev.*, **135**, 3033–3051.

Klemp, J. B. and R. B. Wilhelmson, 1978a: The simulation of three-dimensional convective storm dynamics. *J. Atmos. Sci.*, **35**, 1070–1096.

Klemp, J. B. and R. B. Wilhelmson, 1978b: Simulations of right- and left-moving storms produced through storm splitting. *J. Atmos. Sci.*, **35**, 1097–1110.

Klemp, J. B., R. B. Wilhelmson, and P. S. Ray, 1981: Observed and numerically simulated structure of a mature supercell thunderstorm. *J. Atmos. Sci.*, **38**, 1558–1580.

Klemp, J. B. and Rotunno, R., 1983: A study of the tornadic region within a supercell thunderstorm. J. Atmos. Sci., **40**, 359–377.

Klemp, J. B., 1987: Dynamics of tornadic thunderstorms. *Annu. Rev. Fluid Mech.*, **19**, 369–402.

LaPenta, K. D., Bosart, L.F., Galarneau, T. J., Deckinson, M. J., 2005: A Multiscale Examination of the 31 May 1998 Mechanicville, New York, Tornado. *Wea. Forec.*, **20**, 494-516.

Lemon, L. R. and Doswell III, C. A., 1979: Severe thunderstorm evolution and mesocyclone structure as related to tornadogenesis. *Mon. Wea. Rev.*, **107**, 1184–1197.

Letkewicz, C. E., and M. D. Parker, 2010: Forecasting the maintenance of mesoscale convective systems crossing the Appalachian Mountains. *Wea. Forec.*, **25**, 1179-1195.

Lin, Y.-L., Farley, R. D., and Orville, H. D., 1983: Bulk parameterization of the snow field in a cloud model. J. Clima. Appli. Meteor., **22**, 1065-1092.

Lin, Y.-L., S.-Y. Chen, C.M. Hill, and C.-Y. Huang, 2005: Control parameters for track continuity and deflection associated with tropical cyclones over a mesoscale mountain. *J. Atmos. Sci.*, **62**, 1849–66.

Lin, Y-L., 2007: *Mesoscale Dynamics*. Cambridge University Press, pp. 630.

Markowski, P.M., Dotzek, N, 2011: A numerical study of the effects of orography on supercells. Atmospheric Research, **100**, 457-478.

McCaul, E. W., Jr. and C. Cohen, 2002: The impact on simulated storm structure and intensity of variations in the mixed layer and moist layer depths. *Mon. Wea. Rev.*, **130**, 1722–1748.

McCaul, E. W., Jr. and M. L. Weisman, 2001: The sensitivity of simulated supercell structure and intensity to variations in the shapes of environmental buoyancy and shear profiles. *Mon. Wea. Rev.*, **129**, 664–687.

Miglietta, M.M., and A. Buzzi, 2004: A numerical study of moist stratified flow regimes over isolated topography. Quart. J. Roy. Meteor. Soc., 130, 1749-1770.

Morrison, H., Curry, J. A., and Khvorostyanov, V. I., 2005: A new doublemoment microphysics scheme for application in cloud and climate models. Part 1: Description. J. Atmos. Sci., **62**, 1665–1677.

Newton, C. W. and H. R. Newton, 1959: Dynamical interactions between large convective clouds and environment with vertical shear. *J. Meteor.*, **16**, 483–496.

Parker, M. D., and D. A. Ahijevych, 2007: Convective episodes in the East-Central United States. *Mon. Wea. Rev*., **135**, 3707-3727.

Reeves, H.D., Lin, Y.-L., 2007: The effects of a mountain on the propagation of a preexisting convective system for blocked and unblocked flow regimes. J. Atmos. Sci., **64**, 2401–2421.

Richardson, Y. P., K. K. Droegemeier, and R. P. Davies-Jones, 2007: The influence of horizontal environmental variability on numerically simulated convective storms. Part I: Variations in vertical shear. *Mon. Wea. Rev.*, **135**, 3429–3455.

Rogers, J. C., J. A. Winkler, D. R. Legates, L. O. Mearns, 2006: Climate. In C. J. W. Gary and L. Gaile (Ed.), *Geography in America at the Dawn of the 21st Century* (pp. 32-46). Oxford, NY: Oxford Univ. Press.

Rotunno, R., 1981: On the evolution of thunderstorm rotation. *Mon. Wea. Rev.*, **109**, 577–586.

Rotunno, R. and J. B. Klemp, 1982: The influence of the shear-induced pressure gradient on thunderstorm motion. *Mon. Wea. Rev.*, **110**, 136–151.

Rotunno, R. and J. B. Klemp, 1985: On the rotation and propagation of simulated supercell thunderstorms. *J. Atmos. Sci.*, **42**, 271–292.

Schneider, D. G., 2009: The impact of terrain on three cases of tornadogenesis in the Great Tennessee Valley. *Elec. J. Oper. Meteor.*, EJ11.

Smith, G. M., Lin, Y.-L., and Rastigeyev, Y., 2013: Orographic Effects on Supercell Development, Propagation, and Structure, Atmos. Res., In Review.

Smolarkiewicz, P.K., R. Rotunno, 1989: Low Froude number flow past three-dimensional obstacles. Part I: baroclinically generated lee vortices. *J. Atmos. Sci.*, **46**, 1154–1166.

Sobash, R., Bright, D. R., Dean, A.R., Kain, J.S., Coniglio, M., Weiss, S.J., and Levit, J.J., 2008: Severe storm forecast guidance based on explicit identification of convective phenomena in WRF-model forecasts. *Preprints, 24th Conf. on Severe Local Storms*, Savannah, GA, Amer. Meteor. Soc., 11.3.

van Tassel, E. L., 1955: The North Platte Valley Tornado Outbreak of June 27, 1955. *Mon. Wea. Rev.*, **83**, 255–264.

Thompson, R. L., Edwards, R., Mead, C. M., 2005: An update to the Supercell Composite and Significant Tornado Parameters. Preprints, *22nd Conf. Severe Local Storms*, Hyannis, MA.

Thompson, R. L., Edwards, R., Mead, C. M., 2007: Effective storm-relative helicity and bulk shear in supercell thunderstorm environments. Wea. Forecasting, 22, 102-115.

Weisman, M. L., and J. B. Klemp, 1982 (WK82): The dependence of numerically simulated convective storms on vertical wind shear and buoyancy. *Mon. Wea. Rev.*, **110**, 504–520.

Weisman, M. L. and J. B. Klemp, 1984: The structure and classification of numerically simulated convective storms in directionally varying wind shears. *Mon. Wea. Rev.*, **112**, 2479–2498.

Weisman, M. L., 1993: The genesis of severe, long-lived bow echoes. *J. Atmos. Sci.*, **50**, 645–670.

Wicker, L. J., and Skamarock, W. C., 2002: Time Splitting Methods for Elastic Models Using Forward Time Schemes. Monthly Weather Review, **130**, 2088-2097.

Wicker, L. J. and Wilhelmson, R. B., 1995: Simulation and analysis of tornado development and decay within a three-dimensional supercell thunderstorm. J. Atmos. Sci., **52**, 2675–2703.

Wilhelmson, R. B. and J. B. Klemp, 1978: A numerical study of storm splitting that leads to long-lived storms. *J. Atmos. Sci.*, **35**, 1974–1986.

Witcraft, N. C., Y.-L. Lin, and Y.-H. Kuo, 2005: Dynamics of orographic rain associated with the passage of a tropical cyclone over a mesoscale mountain, *Terr. Atmos. Ocean*, **16**, 1133-1161.

Xue, M., Droegemeier, K.K., Wong, V., Shapiro, A., Brewster, K., Carr, F., Weber, D., Lin, Y., Wang, D., 2001: The Advanced Regional Prediction System (ARPS)—a multi-scale nonhydrostatic atmospheric simulation and prediction model: Part II. Model physics and applications. Meteor. Atmos. Phys., **76**, 143–165.

Ziegler, C.L., E.R. Mansell, J.M. Straka, D.R. MacGorman, D.W. Burgess, 2010: The impact of spatial variations of low-level stability on the life cycle of a simulated supercell storm. *Mon. Wea. Rev.*, **138**, 1738–1766.